YI-RU0781-06

“Smart Bicycle” – based Safety Enhancement for Bicycle/Motorcycle Riding

Final Report
December 2012

Submitted by

Jingang Yi, Ph.D.
Department of Mechanical and Aerospace Engineering and
Center for Advanced Infrastructure and Transportation (CAIT)
Rutgers, The State University of New Jersey
100 Brett Road Piscataway, NJ 08854

and

Yizhai Zhang, Ph.D.
Department of Mechanical and Aerospace Engineering and
Center for Advanced Infrastructure and Transportation (CAIT)
Rutgers, The State University of New Jersey
100 Brett Road Piscataway, NJ 08854

In cooperation with

U.S. Department of Transportation

Federal Highway Administration

Disclaimer Statement

The contents of this report reflect the views of the author(s) who is (are) responsible for the facts and the accuracy of the data presented herein. The contents do not necessarily reflect the official views or policies of the New Jersey Department of Transportation or the Federal Highway Administration. This report does not constitute a standard, specification, or regulation.

The contents of this report reflect the views of the authors, who are responsible for the facts and the accuracy of the information presented herein. This document is disseminated under the sponsorship of the Department of Transportation, University Transportation Centers Program, in the interest of information exchange. The U.S. Government assumes no liability for the contents or use thereof.

TECHNICAL REPORT STANDARD TITLE PAGE

1. Report No.	2. Government Accession No.	3. Recipient's Catalog No.
YI-RU0781-06		

4. Title and Subtitle	5. Report Date
"Smart Bicycle" – based Safety Enhancement for Bicycle/Motorcycle Riding	December 2012
	6. Performing Organization Code: CAIT/Rutgers
7. Author(s): Dr. Jingang Yi and Dr. Yizhai Zhang	8. Performing Organization Report No.: YI-RU0781-06
9. Performing Organization Name and Address: Center for Advanced Infrastructure & Transportation (CAIT), Rutgers, The State University, 100 Brett Rd Piscataway, NJ 08854	10. Work Unit No.
	11. Contract or Grant No.
12. Sponsoring Agency Name and Address: Federal Highway Administration, U.S. Department of Transportation, Washington, D.C.	13. Type of Report and Period Covered: Final Report 7/1/2010-12/31/2012
	14. Sponsoring Agency Code

15. Supplementary Notes

U.S. Department of Transportation/Research and Innovative Technology Administration
1200 New Jersey Avenue, SE
Washington, DC 20590-0001

16. Abstract

Single-track vehicles, such as motorcycles and bicycles, provide an agile mobile platform. Modeling and control of motorcycles for agile maneuvers, such as those by professional racing riders, are challenging due to motorcycle's unstable platform and complex tire/road interaction. This report presents a modeling and tracking control design of autonomous motorcycles/bicycles. We first discuss a new dynamics model for autonomous motorcycles/bicycles. We consider the existence of lateral sliding velocity at the rear wheel contact point. Because of the importance of the tire/road interaction for vehicle stability and maneuverability, the dynamic modeling scheme also includes the motorcycle tires. We then present two designs for trajectory tracking and balancing control of autonomous motorcycles. The first control design is for trajectory tracking and the second design is for path following control (i.e., maneuver regulation control). The both control systems designs are based on the external/internal convertible (EIC) dynamical structure of the motorcycle dynamics. The control design of the EIC systems guarantees an exponential convergence of the motorcycle trajectory to a neighborhood of the desired profiles while the roll motion converges to a neighborhood of the desired equilibria that are estimated for a given desired trajectory. The maneuver regulation control guides the vehicle to follow a desired path and automatically tunes the desired velocity. The velocity field-based maneuver regulation design is integrated with the trajectory tracking controller for motorcycle systems. The effectiveness of the control systems are validated by numerical simulations based on an autonomous motorcycle prototype.

17. Key Words	18. Distribution Statement
Single-track vehicle, nonlinear control, non-minimum phase systems, dynamic inversion.	

19. Security Classif (of this report)	20. Security Classif. (of this page)	21. No of Pages	22. Price
Unclassified	Unclassified	33	

Form DOT F 1700.7 (8-69)

TABLE OF CONTENTS

Page
1.0 Introduction……2

2.0 Motorcycle Dynamics……..4
2.1 Geometry and kinematics relationships……4
2.2 Motorcycle dynamics……6

3.0 Tire Dynamics Models……..8
3.1 Tire kinematics relationships…….. 8
3.2 Modeling of frictional forces……9
3.3 Combined tire and motorcycle dynamics models……10

4.0 Trajectory Tracking Control Systems Design……...11
4.1 External/Internal convertible dynamical systems…… 11
4.2 Trajectory tracking control

4.2.1 Control system overview……...13
4.2.2 Approximate tracking control……13
4.2.3 Estimation of the internal equilibrium…… 15

4.3 Simulation Results……17

5.0 Path-Following Control System Design……..18
5.1 Modeling of tire/road friction forces..……..18
5.2 Combined motorcycle and tire dynamics model……19
5.3 Path-Following Maneuvering Design……..20

5.3.1 Time suspension and velocity field design……..20
5.3.2 Controller Design……21

5.4 Simulation Results……..21

6.0 Conclusion……..25

"Smart Bicycle"*

Yizhai Zhang† and Jingang Yi‡

Department of Mechanical and Aerospace Engineering, and
Center for Advanced Infrastructure and Transportation
Rutgers, The State University of New Jersey
Piscataway, New Jersey 08854, USA

Abstract

Single-track vehicles, such as motorcycles and bicycles, provide an agile mobile platform. Modeling and control of motorcycles for agile maneuvers, such as those by professional racing riders, are challenging due to motorcycle's unstable platform and complex tire/road interaction. This report presents a modeling and tracking control design of autonomous motorcycles/bicycles. We first discuss a new dynamics model for autonomous motorcycles/bicycles. We consider the existence of lateral sliding velocity at the rear wheel contact point. Because of the importance of the tire/road interaction for vehicle stability and maneuverability, the dynamic modeling scheme also includes the motorcycle tires. We then present two designs for trajectory tracking and balancing control of autonomous motorcycles. The first control design is for trajectory tracking and the second design is for path following control (i.e., maneuver regulation control). The both control systems designs are based on the external/internal convertible (EIC) dynamical structure of the motorcycle dynamics. The control design of the EIC systems guarantees an exponential convergence of the motorcycle trajectory to a neighborhood of the desired profiles while the roll motion converges to a neighborhood of the desired equilibria that are estimated for a given desired trajectory. The maneuver regulation control guides the vehicle to follow a desired path and automatically tunes the desired velocity. The velocity field-based maneuver regulation design is integrated with the trajectory tracking controller for motorcycle systems. The effectiveness of the control systems are validated by numerical simulations based on an autonomous motorcycle prototype.

Keywords: Single-track vehicle, nonlinear control, non-minimum phase systems, dynamic inversion,

Nomenclature

X, Y, Z	A ground-fixed coordinate system.
x, y, z	A wheel-base line moving coordinate system.
x_w, y_w, z_w	A front wheel plane coordinate system.
x_B, y_B, z_B	A rear frame body coordinate system.
C_1, C_2	Front and rear wheel contact points on the ground.
F_{fx}, F_{fy}, F_{fz}	The front wheel contact forces in the x, y, z-axis directions.
F_{rx}, F_{ry}, F_{rz}	The rear wheel contact forces in the x, y, z directions.
$\boldsymbol{v}_f, \boldsymbol{v}_r$	Velocity vectors of the front and rear wheel contact points, respectively.
v_{fx}, v_{fy}	Front wheel contact point C_1 velocities along the x- and y-axis directions, respectively.
v_{rx}, v_{ry}	Rear wheel contact point C_2 velocities along the x- and y-axis directions, respectively.
v_{fx_w}, v_{fy_w}	Front wheel contact point C_1 velocities along the x_w- and y_w-axis directions, respectively.
v_X, v_Y	Rear wheel contact point C_2 velocities along the X- and Y-axis directions, respectively.

*Research supported by Rutgers Center for Advanced Infrastructure and Transportation.

†Graduate student; Email: yzzhang@eden.rutgers.edu.

‡Assistant Professor and corresponding author; Email: jgyi@rutgers.edu, Tel: 1-848-445-3282, Fax: 1-732-445-3124.

ω_f, ω_r	Wheel angular velocities of the front and rear wheels, respectively.
$\boldsymbol{v}_G$	Velocity vector of the motorcycle frame (with rear wheel set).
γ_f, γ_r	Slip angles of the front and rear wheels, respectively.
λ_f, λ_r	Longitudinal slip values of the front and rear wheels, respectively.
φ, ψ	Rear frame roll and yaw angles, respectively.
φ_f	The front steering wheel plane camber angle.
ϕ	Motorcycle steering angle.
ϕ_g	Motorcycle kinematic steering angle (projected steering angle on the ground plane).
σ	The front kinematic steering angle variable.
m	The total mass of the motorcycle rear frame and wheel.
J_s	The mass moment of rotation of the steering fork (with the front wheel set) about its rotation axis.
l	Motorcycle wheel base, i.e., distance between C_1 and C_2.
l_t	The front steering wheel trail.
h	The height of the motorcycle center of mass.
r	The front and rear wheel radius.
δ	The rear frame rotation angle from its vertical position.
ξ	The front steering axis caster angle.
R	The radius of the trajectory of point C_2 under neutral steering turns.
C_d	The aerodynamics drag coefficient.
k_λ, k_γ, k_φ	Longitudinal, lateral, and camber stiffness coefficients of motorcycle tires, respectively.
$L(L_c)$	The (constrained) Lagrangian of the motorcycle systems.

1 Introduction

Single-track vehicles, such as motorcycles and bicycles, have high maneuverability and strong off-road capabilities. In environments such as deserts, forests, and mountains, mobility of single-track vehicles significantly outperforms that of double-track vehicles. The recent demonstration of the Blue Team's autonomous motorcycle in the 2005 DARPA Grand Challenge autonomous ground vehicles competition has shown an example of the high-agility of the single-track platform [1]. Although the extensive study of the motorcycle dynamics have revealed the performance under steady motions, however, modeling and control of motorcycles for agile maneuvers, such as those by professional racing riders, still remains a challenging task due to motorcycle's intrinsic unstable platform and complex tire/road interaction. Professional motorcycle riders can leverage the safety limits of the tire/road interaction, and maintain the vehicles at high performance while preserving safety. The goal of this work is to develop a new modeling and control scheme for an autonomous motorcycle.

Mathematically modeling of a bicycle or a motorcycle has been an active research area for many years. Although some modeling differences have been discussed in [2], from control system design aspects, we consider bicycles and motorcycles are similar, and hence do not explicitly distinguish them. There is a large body of work that studies motorcycle stability and dynamics, and readers can refer to two recent review papers: one from a historical development viewpoint [2] and the other from a control-oriented perspective [3]. The modeling work can be considered as two groups [3]: a simple inverted pendulum model and a multi-body dynamic model. For example, some simple second-order dynamic models are presented in [4] to study the balance stability of a bicycle. Several researchers have studied the motorcycle dynamics using multi-body dynamics [5–8]. The model developed in [6] is very comprehensive and contains various vehicle components. The model has been implemented in a simulation package called *FastBike* for the purposes of real-time simulations. Multi-body

dynamics models are not suitable for the control system design due to their complexity while a inverted-pendulum model overly simplify the problem and does not capture all of the dynamics and geometric characteristics.

In [9, 10], mathematical models of a motorcycle are discussed using (constrained) Lagrange's equations. In [11], experimental study of the motorcycle handling is compared with the mathematical dynamics model of a motorcycle with the rider. Stability and steering characteristics of a motorcycle are typically discussed using a linearization approach with a consideration of a constant velocity [2, 3, 5, 12–15]. A *non-minimum phase* property (unstable poles and zeros) in these analyses explains the counter-steering phenomena and other steering stability observations. In [12], it is also demonstrated experimentally the in-significance of the gyroscopic effect of the front wheel. The concept of an autonomous bicycle without a rider has been proposed by several researchers [1, 9, 16–20]. In this work, we extend the modeling and control design in [9, 16]. For the modeling part, we take a constrained Lagrangian approach to capture the nonlinear dynamics of a motorcycle. Besides the consideration of control-oriented modeling approach that captures the fundamental properties of the motorcycle platform with a manageable complexity, several new features have been adopted and developed. First, we relax the zero lateral velocity of the wheel contact points and therefore allow wheel sliding in the models, which provides more realistic vehicle modeling [2]. Second, we explicitly consider the tire/road interaction for designing control algorithms because of the importance of the tire/road interaction on motorcycle dynamics [21]. The study in [22] is probably the closest work to ours. The authors in [22] employ a nonholonomic motorcycle dynamics and focus on the performance and maneuverability analysis of motorcycles using the automotive tire/road interaction characteristics.

Control of an autonomous motorcycle only using the steering and vehicle velocity as inputs is challenging due to the platform's non-minimum phase and underactuation properties [1]. For such systems, there does not exist an analytical casual compensator for *exactly* output tracking while keeping the internal stability [26]. With an extra rider lean as an control input, it has been shown that maneuvering a bicycle becomes easier because adding the extra control input essentially eliminates the right half-plane zeros [3]. In [17], an autonomous bicycle is designed and balanced using gyroscopic actuators. The controller in [17] is based on a linearized bicycle model. In [9], a nonlinear control method is designed for a trajectory tracking and balancing. In [18], a balancing and tracking control mechanism is designed by on-board shifting weights. In [19, 20], a simplified inverted pendulum model is utilized for bicycle balancing. A proportional derivative (PD) controller with a disturbance observer is employed to balance the bicycle. The authors however focus on balancing the bicycle on a straight-line motion. We employ and extend the control design in [9, 16]. In [9], an external/internal convertible (EIC) dynamical system is presented and the motorcycle dynamics are of an example of the EIC systems. A nonlinear tracking control design is also discussed for the non-minimum phase bicycle dynamic systems. In our previous work [16], we have extended the dynamic models to consider motorcycle geometric and steering mechanism properties. In [9, 16], nonholonomic constraints of zero lateral velocity at the rear wheel contact point are enforced and only rear wheel friction force is considered for traction/braking forces. The control systems design takes advantages of the control actuation flexibility and reduces the design complexity than those in [9, 16]. Two simulation examples demonstrate the effectiveness and efficacy of the control systems design.

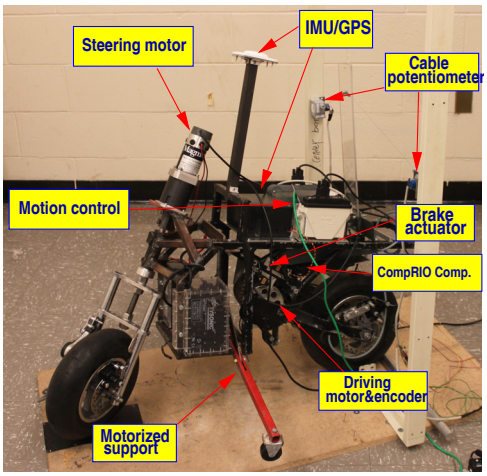

Figure 1: A Rutgers autonomous pocket bike.

Besides the EIC trajectory tracking control design, we also present a path-following design to overcome the large errors shown in the trajectory tracking. For autonomous vehicles, particularly the underactuated mechanical systems, maneuver regulation or path following control has demonstrated a superior performance comparing

[1] An underactuated mechanical system is referred to a mechanical dynamic system in which the number of control inputs is less than the number of the generalized coordinates [24]. Readers can also refer to [25] for an overview of control of nonlinear non-minimum phase systems.

with pre-specified trajectory tracking in time domain [27–31]. In those maneuver regulation design, the desired velocity profile along the trajectory is obtained either using Lyapunov-based approach (e.g., [31]) or requiring online solving an optimization problem (e.g., [31]), which is non-causal for non-minimum phase dynamical systems such as motorcycle dynamics. We use a velocity field concept to generate the desired velocity profile for motorcycle systems. Our approach is inspired by the work in [32] of passivity-based control of fully-actuated robot manipulators. We integrate the velocity field concept with the EIC control design of underactuated non-minimum phase motorcycle dynamics. The presented trajectory tracking and path-following control design are extension of the work presented in the conference papers [33, 34].

Comparing with existing study on the motorcycle dynamics and control, the main contribution of this study is the new modeling and control system design with integrated motorcycle dynamics with tire/road interaction. First, we do not enforce a zero lateral velocity nonholonomic constraint for the wheel contact points of the motorcycle system. Such nonholonomic constraints are not realistic for high-fidelity vehicle modeling [2]. Second, we explicitly consider the tire/road interaction for designing control algorithms because of the importance of the tire/road interaction on motorcycle dynamics. To our knowledge, there is no study that explicitly considers such kinds of tire dynamics into the motorcycle control system design. The presented work here is an extension of the work in [23]. Based on the new dynamics, we extend the control system design in [9, 16] for trajectory tracking and path-following maneuvers.

The remainder of the report is organized as follows. In Section 2, we discuss dynamic modeling of a riderless motorcycle. In Section 3, we present a motorcycle tire dynamics model and then integrate the tire dynamics with the motorcycle dynamics. In Section 4, we present an EIC-based tracking and balancing control design. We then present a tracking error improvement by path-following control design in Section 5. Both trajectory-tracking and path-following control designs are validated through simulation results. Finally, we conclude the report and discuss future research directions in Section 6.

2 Motorcycle Dynamics

Fig. 1 shows the Rutgers autonomous motorcycle prototype. The motorcycle is rear-wheel driving and steering and velocity control are the control inputs. We do not use the weight shifting as one actuation mechanism as human riders do because it has been demonstrated an effective maneuverability only through vehicle steering and velocity control [1].

2.1 Geometry and kinematics relationships

The riderless motorcycle is considered as as a two-part platform: a rear frame and a steering mechanism. Fig. 2(a) shows a schematic of the vehicle. We consider the following modeling assumptions: (1) the wheel/ground is a point contact and thickness and geometry of the motorcycle tire are neglected; (2) The motorcycle body frame is considered a point mass; and (3) the motorcycle moves on a flat plane and vertical motion is neglected, namely, no suspension motion.

We denote C_1 and C_2 as the front and rear wheel point points with the ground, respectively. As illustrated in Fig. 2(a), three coordinate systems are used: the navigation frame $\mathcal{N}$ (X, Y, Z-axis fixed on the ground), the wheel base moving frame (x, y, z-axis fixed along line C_1C_2), and the rear body frame $\mathcal{B}$ (x_B, y_B, z_B-axis fixed on the rear frame). For frame $\mathcal{B}$, we use (3-1-2) Euler angles and represent the motion by the yaw angle ψ and roll angle φ. We denote the unit vector sets for the three coordinate systems as $(\boldsymbol{I}, \boldsymbol{J}, \boldsymbol{K})$, $(\boldsymbol{i}, \boldsymbol{j}, \boldsymbol{k})$, and $(\boldsymbol{i}_B, \boldsymbol{j}_B, \boldsymbol{k}_B)$, respectively. It is straightforward to obtain that

$$\begin{bmatrix} \boldsymbol{i}_B \\ \boldsymbol{j}_B \\ \boldsymbol{k}_B \end{bmatrix} = \left[\begin{array}{c:c} 1 & \mathbf{0} \\ \hdashline \mathbf{0} & \boldsymbol{R}(\varphi) \end{array}\right] \begin{bmatrix} \boldsymbol{i} \\ \boldsymbol{j} \\ \boldsymbol{k} \end{bmatrix} = \left[\begin{array}{c:c} 1 & \mathbf{0} \\ \hdashline \mathbf{0} & \boldsymbol{R}(\varphi) \end{array}\right] \left[\begin{array}{c:c} \boldsymbol{R}(\psi) & \mathbf{0} \\ \hdashline \mathbf{0} & 1 \end{array}\right] \begin{bmatrix} \boldsymbol{I} \\ \boldsymbol{J} \\ \boldsymbol{K} \end{bmatrix} = \begin{bmatrix} \mathrm{c}_\psi & \mathrm{s}_\psi & 0 \\ -\mathrm{c}_\varphi \mathrm{s}_\psi & \mathrm{c}_\varphi \mathrm{c}_\psi & \mathrm{s}_\varphi \\ \mathrm{s}_\varphi \mathrm{s}_\psi & -\mathrm{s}_\varphi \mathrm{c}_\psi & \mathrm{c}_\varphi \end{bmatrix} \begin{bmatrix} \boldsymbol{I} \\ \boldsymbol{J} \\ \boldsymbol{K} \end{bmatrix}, \quad (1)$$

where the rotation matrix

$$\boldsymbol{R}(x) = \begin{bmatrix} \mathrm{c}_x & \mathrm{s}_x \\ -\mathrm{s}_x & \mathrm{c}_x \end{bmatrix}$$

and $\mathrm{c}_x := \cos x$, $\mathrm{s}_x := \sin x$ for angle x.

We consider the trajectory of point C_2, denoted by its coordinates (X, Y) in $\mathcal{N}$, as the motorcycle position. The orientation of the coordinate systems and the positive directions for angles and velocities follow the conversion of the SAE standard [15]. We consider the instantaneous rotation center of the motorcycle motion on the horizontal plane. Let O_r denote the instantaneous rotation center and O'_r denote the neutral instantaneous rotation center which is the intersection point of the perpendicular lines of the front and rear wheel planes; see Fig. 2. Under the neutral turning condition [7], the slip angles of the front and rear wheels are the same, that is, $\lambda_f = \lambda_r$, and then the rotation center angles for O_r and O'_r are equal to the kinematic steering angle ϕ_g, namely, $\alpha = \alpha' = \phi_g$. Let R denote the instantaneous radius of the trajectory of point C_2 under neutral turning conditions. We define σ as the kinematic steering variable as

$$\sigma := \tan \phi_g = \frac{l}{R} \,. \tag{2}$$

From the geometry of the front wheel steering mechanism [7], we find the following relationship,

$$\tan \phi_g \, \mathrm{c}_\varphi = \tan \phi \, \mathrm{c}_\xi \ . \tag{3}$$

If we assume a small roll and steering angles, then from (3) we obtain an approximation

$$\dot{\sigma} \, \mathrm{c}_\varphi = \dot{\phi} \, \mathrm{c}_\xi \,. \tag{4}$$

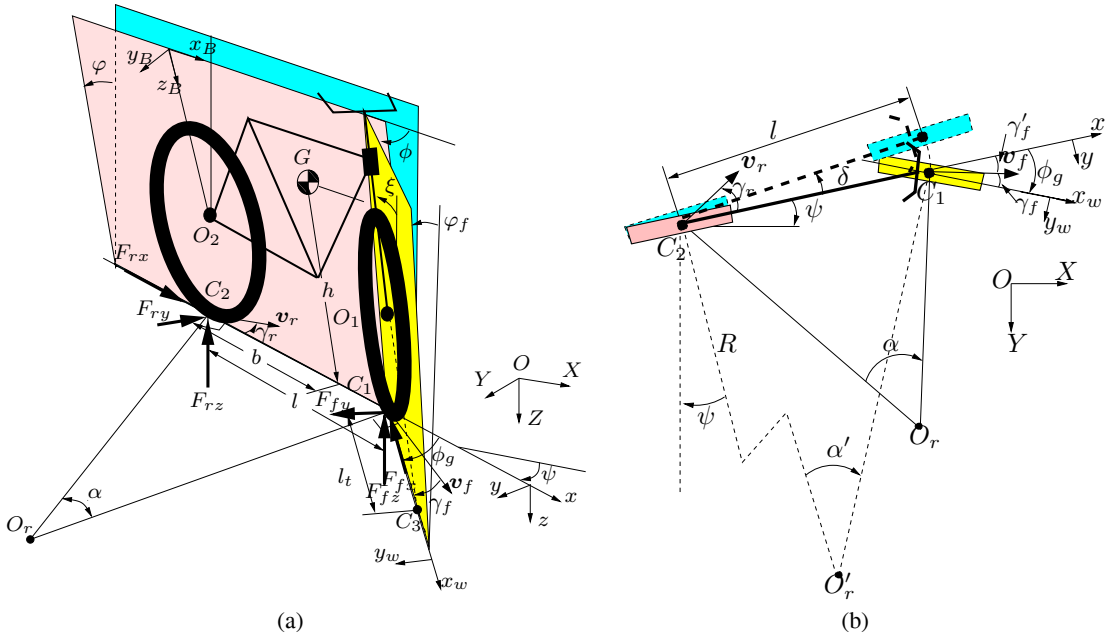

Figure 2: A schematic of the riderless motorcycle/bicycle. (a) Kinematic and dynamic modeling schematic. (b) Top view of the motorcycle/bicycle kinematic steering mechanism.

The motion of the motorcycle on the XY plane is captured by the generalized coordinates $(X, Y, \psi, \varphi, \sigma)$. Note that the use of variable σ is to capture the steering impact on the motorcycle dynamics. The nonholonomic constraint of the rear wheel and the motion trajectory geometry imply the yaw kinematics equality

$$v_{rx} = R\dot{\psi} = \frac{l}{\sigma}\dot{\psi} \,. \tag{5}$$

From a differential geometry viewpoint [2], we can partition the generalized velocities of the motorcycle as base velocities $\dot{\boldsymbol{r}} = [\dot{\varphi},\, v_{rx},\, v_{ry},\, \dot{\sigma}]^T$ and fiber velocities $\dot{\boldsymbol{s}} = \dot{\psi}$. We then write the constraints in (5) simply as

$$\dot{\boldsymbol{s}} + A(\boldsymbol{r}, \boldsymbol{s})\dot{\boldsymbol{r}} = 0, \tag{6}$$

[2] We here take a description of the base-fiber structure of nonholonomic dynamical systems with symmetry in [35].

where $A(\boldsymbol{r}, \boldsymbol{s}) = \begin{bmatrix} 0 & -\frac{\sigma}{l} & 0 & 0 \end{bmatrix}$.

Due to the steering mechanism and caster angle, the height of the mass center of gravity of the motorcycle is changing under steering. As shown in Fig. 2(b), the height change Δh_G of the center of gravity G due to the steering action can be calculated as [16]

$$\Delta h_G = \delta b \, \mathrm{s}_\varphi \approx \frac{b l_t \sigma \, \mathrm{c}_\xi}{l} \, \mathrm{s}_\varphi \,, \tag{7}$$

where we use a small angle approximation $\sigma \approx \phi_g$ from the relationship (2).

Remark 1 *The height change Δh_G of the gravity center G due to steering given in (7) is an approximation. A more accurate modeling of Δh_G with experimental validation is given in [36]. The model of Δh_G given in [36] considers the effect of the tire size without using a small angle approximation and the resultant relationship between Δh_G and s_φ is not linear as shown in (7). However, we still use the simplified model (7) to design the trajectory tracking and path-following controllers in Section 4 and the results can be straightforward extended to the realistic steering model in [36].*

Remark 2 *In [9, 22], the steering axis is assumed to be vertical. This assumption simplifies the motorcycle dynamics and neglects a significant geometric stabilization mechanism, which is the "motorcycle trail" (denoted as l_t in Fig. 2(a)) discussed in [4, 7, 12, 13]. The resulting model of the motorcycle dynamics cannot capture the influence of the steering angle ϕ on the roll dynamics when $v_{rx} = 0$. Namely, one cannot use steering to stabilize the motorcycle. Such an observation is also pointed out in [3].*

Given roll angle φ and steering angle ϕ, the camber angle of the front wheel is approximated as [7]

$$\varphi_f = \varphi + \phi \, \mathrm{s}_\xi \,. \tag{8}$$

We consider the relationship between velocities of the rear wheel contact point C_2 and the front wheel center O_1. We write the position vector $\boldsymbol{r}_{O_1} = \boldsymbol{r}_{C_2} + \boldsymbol{\rho}_{C_2O_1}$, where $\boldsymbol{r}_{C_2}$ is the position vector of point C_2 and $\boldsymbol{\rho}_{C_2O_1} = l\boldsymbol{i}_B - r\boldsymbol{k}_B = l\boldsymbol{i} + r\,\mathrm{s}_\varphi \boldsymbol{j} - r\,\mathrm{c}_\varphi \boldsymbol{k}$ is the relative position vector of G. The angular velocity of the rear frame is represented as $\boldsymbol{\omega} = \dot{\varphi}\boldsymbol{i} + \dot{\psi}\boldsymbol{k}$. Thus, we obtain

$$\boldsymbol{v}_{O_1} = \dot{\boldsymbol{r}}_{C_2} + \boldsymbol{\omega} \times \boldsymbol{\rho}_{C_2O_1} = (v_{rx} - r\dot{\psi}\,\mathrm{s}_\varphi)\boldsymbol{i} + (v_{ry} + l\dot{\psi} + r\dot{\varphi}\,\mathrm{c}_\varphi)\boldsymbol{j} + r\dot{\varphi}\,\mathrm{s}_\varphi \boldsymbol{k}. \tag{9}$$

2.2 Motorcycle dynamics

We use the constrained Lagrangian method in [35] to obtain the dynamics equation of the motion of the riderless motorcycle. We consider the motorcycle as two parts: one rear frame with mass m and one steering mechanism with the mass moment of inertia J_s. The Lagrangian L of the motorcycle is calculated as

$$L = \frac{1}{2} J_s \dot{\phi}^2 + \frac{1}{2} m \boldsymbol{v}_G \cdot \boldsymbol{v}_G - mg\,(h\,\mathrm{c}_\varphi - \Delta h_G) \tag{10}$$

To calculate the mass center velocity, we take a similar approach as in (9) and obtain

$$\boldsymbol{v}_G = (v_{rx} - h\dot{\psi}\,\mathrm{s}_\varphi)\boldsymbol{i} + (v_{ry} + b\dot{\psi} + h\dot{\varphi}\,\mathrm{c}_\varphi)\boldsymbol{j} + h\dot{\varphi}\,\mathrm{s}_\varphi \boldsymbol{k}.$$

Plugging the above equations and (4)-(7) into (10), we obtain

$$L = \frac{J_s}{2\,\mathrm{c}_\xi^2}\dot{\sigma}^2 + \frac{1}{2} m \left[(v_{rx} - h\dot{\psi}\,\mathrm{s}_\varphi)^2 + (v_{ry} + b\dot{\psi} + h\dot{\varphi}\,\mathrm{c}_\varphi)^2 + h^2\dot{\varphi}^2\,\mathrm{s}_\varphi^2 \right] - mg\left(h\,\mathrm{c}_\varphi - \frac{b l_t\,\mathrm{c}_\xi}{l}\sigma\,\mathrm{s}_\varphi \right). \tag{11}$$

Incorporating the constraints (6), we obtain the constrained Lagrangian L_c as [3]

$$L_c = \frac{J_s}{2\,\mathrm{c}_\xi^2}\,\mathrm{c}_\varphi^2\,\dot{\sigma}^2 + \frac{1}{2}m\Bigg\{\left[\left(1-\frac{h}{l}\sigma\,\mathrm{s}_\varphi\right)^2+\frac{b^2}{l^2}\sigma^2\right]v_{rx}^2 + v_{ry}^2 + \frac{2b}{l}\sigma v_{rx}v_{ry} + \frac{2bh}{l}\,\mathrm{c}_\varphi\,\sigma\dot{\varphi}v_{rx} + 2h\,\mathrm{c}_\varphi\,\dot{\varphi}v_{ry} + h^2\dot{\varphi}^2\Bigg\} - mg\left(h\,\mathrm{c}_\varphi - \frac{bl_t\,\mathrm{c}_\xi}{l}\sigma\,\mathrm{s}_\varphi\right). \tag{12}$$

The moment M_s on the rotating axis is obtained as

$$M_s = \frac{l_t}{\sqrt{1+(l_t/r)^2}}\left(F_{fy}\,\mathrm{c}_{\varphi_f} - F_{fz}\,\mathrm{s}_{\varphi_f}\right). \tag{13}$$

The detailed calculation of (13) is given in Appendix A.

The equations of motion using the constrained Lagrangian are obtained as [35] [4]

$$\frac{d}{dt}\frac{\partial L_c}{\partial \dot{r}^i} - \frac{\partial L_c}{\partial r^i} + A_i^k\frac{\partial L_c}{\partial s^k} = -\frac{\partial L}{\partial \dot{s}^l}C_{ij}^l\dot{r}^j + \tau^i,\ i,j=1,\ldots,4, \tag{14}$$

where τ^i are the external forces/torques, A_i^k is the element of connection $A(\boldsymbol{r},\boldsymbol{s})$ at the kth row and ith column, and C_{ij}^l denote the components of the curvature of $A(\boldsymbol{r},\boldsymbol{s})$ as

$$C_{ij}^l = \frac{\partial A_i^l}{\partial r^j} - \frac{\partial A_j^l}{\partial r^i} + A_i^k\frac{\partial A_j^l}{\partial s^k} - A_j^k\frac{\partial A_i^l}{\partial s^k}. \tag{15}$$

From state variable σ, from (14), we obtain the steering dynamics as

$$\frac{d}{dt}\left(\frac{J_s}{\mathrm{c}_\xi^2}\,\mathrm{c}_\varphi^2\,\dot{\sigma}\right) - \frac{mgl_tb\,\mathrm{c}_\xi}{l}\,\mathrm{s}_\varphi = \tau_s + M_s\,. \tag{16}$$

Considering a position feedback control of the steering angle directly, we can reduce the dynamic equation (16) by a kinematic steering system as

$$\dot{\sigma} = \omega_\sigma, \tag{17}$$

where the input ω_σ is considered as the virtual steering velocity and given by dynamic extension

$$\dot{\omega}_\sigma = \frac{\mathrm{c}_\xi^2}{J_s\,\mathrm{c}_\varphi^2}\left(\tau_s + M_s\right) - 2\tan\varphi\dot{\varphi}\dot{\sigma} + \frac{mgl_tb\,\mathrm{c}_\xi^3}{lJ_s}\,\mathrm{s}_\varphi\,.$$

Similarly, we obtain the roll dynamics equation

$$\frac{bh\sigma}{l}\mathrm{c}_\varphi\,\dot{v}_{rx} + h\,\mathrm{c}_\varphi\,\dot{v}_{ry} + h^2\ddot{\varphi} + \left(1-\frac{h\sigma}{l}\,\mathrm{s}_\varphi\right)\frac{h\sigma\,\mathrm{c}_\varphi}{l}v_{rx}^2 - g\left(h\,\mathrm{s}_\varphi + \frac{l_tb\,\mathrm{c}_\xi}{l}\sigma\,\mathrm{c}_\varphi\right) = -\frac{bh}{l}\,\mathrm{c}_\varphi\,v_{rx}\omega_\sigma, \tag{18}$$

longitudinal dynamics equation

$$\left[\left(1-\frac{h\sigma}{l}\,\mathrm{s}_\varphi\right)^2+\frac{b^2\sigma^2}{l^2}\right]\dot{v}_{rx} + \frac{b\sigma}{l}\dot{v}_{ry} + \frac{bh\sigma}{l}\,\mathrm{c}_\varphi\,\ddot{\varphi} - 2\Big(1-\frac{h\sigma}{l}\,\mathrm{s}_\varphi\Big)\frac{h\sigma}{l}\,\mathrm{c}_\varphi\,\dot{\varphi}v_{rx} - \frac{bh\sigma}{l}\,\mathrm{s}_\varphi\,\dot{\varphi}^2 = -\Bigg[-2\Big(1-\frac{h\sigma}{l}\mathrm{s}_\varphi\Big)\frac{h}{l}\,\mathrm{s}_\varphi\,v_{rx} + \frac{2b^2\sigma}{l^2}v_{rx} + \frac{b}{l}v_{ry} + \frac{bh}{l}\,\mathrm{c}_\varphi\,\dot{\varphi}\Bigg]\omega_\sigma + \frac{1}{m}F_{rx} - \frac{1}{m\sqrt{1+\sigma^2}}\left(F_{fx}+\sigma F_{fy}\right) - \frac{1}{m}C_dv_{rx}^2, \tag{19}$$

[3] Readers can refer to [35] for the definition of the constrained Lagrangian L_c and also Chapter 5 of [35] for the Lagrange-d'Alembert principle for nonholonomic constrained dynamical systems.

[4] Here the summation convention is used where, for example, if s is of dimension m, then $A_i^k\frac{\partial A_j^l}{\partial s^k} \equiv \Sigma_{k=1}^m A_i^k\frac{\partial A_j^l}{\partial s^k}$.

and lateral dynamics equation

$$\frac{b\sigma}{l}\dot{v}_{rx}+\dot{v}_{ry}+h\,\mathrm{c}_\varphi\,\ddot{\varphi}-h\,\mathrm{s}_\varphi\,\dot{\varphi}^2=-\frac{bv_{rx}}{l}\omega_\sigma-\frac{1}{m}F_{ry}+\frac{1}{m\sqrt{1+\sigma^2}}\left(F_{fy}-\sigma F_{fx}\right). \tag{20}$$

In (19), C_d is the aerodynamic drag coefficient.

Let $\dot{\boldsymbol{q}}:=[\dot{\varphi}\ v_{rx}\ v_{ry}]^T$ denote the generalized velocity of the motorcycle and we rewrite the above dynamics equations (18)-(20) in a compact matrix form as

$$\mathbf{M}\ddot{\boldsymbol{q}}=\mathbf{K}_m+\mathbf{B}_m\begin{bmatrix}\omega_\sigma\\F_{fx}\\F_{fy}\\F_{rx}\\F_{ry}\end{bmatrix}, \tag{21}$$

where matrices

$$\mathbf{M}=\begin{bmatrix}M_{11}&M_{12}\\M_{21}&M_{22}\end{bmatrix}=\left[\begin{array}{c:cc}h^2&\frac{bh\sigma}{l}\,\mathrm{c}_\varphi&h\,\mathrm{c}_\varphi\\\hdashline\frac{bh\sigma}{l}\,\mathrm{c}_\varphi&\left(1-\frac{h\sigma}{l}\,\mathrm{s}_\varphi\right)^2+\frac{b^2\sigma^2}{l^2}&\frac{b\sigma}{l}\\h\,\mathrm{c}_\varphi&\frac{b\sigma}{l}&1\end{array}\right], \tag{22}$$

$$\mathbf{K}_m=\begin{bmatrix}-\left(1-\frac{h\sigma}{l}\,\mathrm{s}_\varphi\right)\frac{h\sigma\,\mathrm{c}_\varphi\,v_{rx}^2}{l}+g\left(h\,\mathrm{s}_\varphi+\frac{l_t b\,\mathrm{c}_\xi\,\sigma\,\mathrm{c}_\varphi}{l}\right)\\\left(1-\frac{h\sigma\,\mathrm{s}_\varphi}{l}\right)\frac{2h\sigma\,\mathrm{c}_\varphi\,\dot{\varphi}v_{rx}}{l}+\frac{bh\sigma\,\mathrm{s}_\varphi\,\dot{\varphi}^2}{l}-\frac{C_d v_{rx}^2}{m}\\h\,\mathrm{s}_\varphi\,\dot{\varphi}^2\end{bmatrix},\ \mathbf{B}_m=\begin{bmatrix}\frac{-bh\,\mathrm{c}_\varphi\,v_{rx}}{l}&0&0&0&0\\B_\omega&\frac{-1}{m\sqrt{1+\sigma^2}}&\frac{-\sigma}{m\sqrt{1+\sigma^2}}&\frac{1}{m}&0\\\frac{-bv_{rx}}{l}&\frac{-\sigma}{m\sqrt{1+\sigma^2}}&\frac{1}{m\sqrt{1+\sigma^2}}&0&\frac{-1}{m}\end{bmatrix}.$$

In the above matrix $\mathbf{B}_m$, $B_\omega=2\left[\left(1-\frac{h\sigma}{l}\,\mathrm{s}_\varphi\right)\frac{h}{l}\,\mathrm{s}_\varphi-\frac{b^2\sigma}{l^2}\right]v_{rx}-\frac{b}{l}v_{ry}-\frac{bh}{l}\,\mathrm{c}_\varphi\,\dot{\varphi}$. It is clear that the control inputs in (17) and (21) are the virtual steering velocity ω_σ and the wheel traction/braking forces $\boldsymbol{F}_f$ and $\boldsymbol{F}_r$.

3 Tire Dynamics Models

In this section, we discuss how to capture the motorcycle tire/road interaction. We particularly like to present a friction forces modeling scheme for motorcycle dynamics (21).

3.1 Tire kinematics relationships

Fig. 3 illustrates the kinematics of the tire/road contact. Let $\boldsymbol{v}_c=v_{cx}\boldsymbol{i}+v_{cy}\boldsymbol{j}+v_{cz}\boldsymbol{k}$ and $\boldsymbol{v}_o=v_{ox}\boldsymbol{i}+v_{oy}\boldsymbol{j}+v_{oz}\boldsymbol{k}$ denote the velocities of the contact point and the wheel center in the frame $\mathcal{B}$, respectively. We define the longitudinal slip ratio λ_s and lateral side slip ratio λ_γ, respectively, as

$$\lambda_s:=\frac{v_{cx}-r\omega_w}{v_{cx}},\ \lambda_\gamma:=\tan\gamma=-\frac{v_{cy}}{v_{cx}}, \tag{23}$$

where ω_w is the wheel angular velocity and γ is the side slip angle.

For the front wheel, the camber angle is different (8), and the velocity relationship between C_1 and the wheel center O_1 in $\mathcal{B}$ is then

$$v_{fx}=v_{fox}+r\dot{\psi}\,\mathrm{s}_\varphi,\ v_{fcy}=v_{foy}-r\dot{\varphi}_f\,\mathrm{c}_\varphi,\ v_{fz}=v_{foz}-r\dot{\varphi}_f\,\mathrm{s}_\varphi. \tag{24}$$

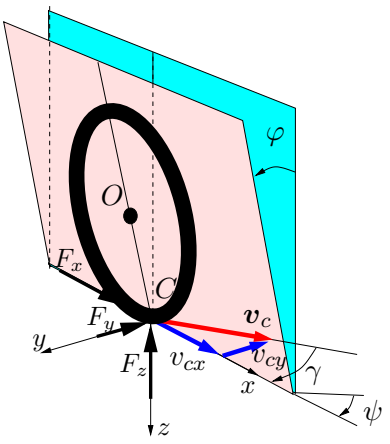

Figure 3: Schematic of the tire kinematics.

Using the relationship (9) and (8), we simplify the above velocity calculation and obtain

$$v_{fx} = v_{rx},\ v_{fy} = v_{ry} - r\dot{\phi}\,\mathrm{s}_\xi\,\mathrm{c}_\varphi + l\dot{\psi}. \tag{25}$$

From the side slip ratio (23) of the rear wheel, we have

$$\lambda_{r\gamma} = \tan\gamma_r = -\frac{v_{ry}}{v_{rx}} = -\frac{v_{fy}}{v_{fx}} - \frac{r\dot{\phi}\,\mathrm{s}_\xi\,\mathrm{c}_\varphi - l\dot{\psi}}{v_{rx}} = \tan\gamma_f' - \frac{r\tan\xi\,\mathrm{c}_\varphi^2}{v_{rx}}\omega_\sigma + \sigma, \tag{26}$$

where $\gamma_f' := \phi_g - \gamma_f$ and $\tan\gamma_f' = -\frac{v_{fy}}{v_{fx}}$; see Fig. 2. We also use relationships (4) and (5) in the last step above. Moreover, from (2) and the geometry and kinematics of the front wheel (Fig. 2), we have

$$\sigma = \tan\phi_g = \tan(\gamma_f' + \gamma_f) \approx \tan\gamma_f' + \tan\gamma_f = \lambda_{r\gamma} + \frac{r\tan\xi\,\mathrm{c}_\varphi^2}{v_{rx}}\omega_\sigma - \sigma + \lambda_{f\gamma}.$$

Therefore, we obtain the relationship between the front and rear wheel side slip ratios as follows.

$$\lambda_{f\gamma} = 2\sigma - \frac{r\tan\xi\,\mathrm{c}_\varphi^2}{v_{rx}}\omega_\sigma - \lambda_{r\gamma}. \tag{27}$$

Similarly, we can obtain the slip ratio calculation of the front wheel as follows. First, we obtain the longitudinal velocity of the contact point C_1 as

$$v_{fx_w} = v_{fx}\,\mathrm{c}_{\phi_g} + v_{fy}\,\mathrm{s}_{\phi_g} \approx v_{rx}\,\mathrm{c}_{\phi_g} + (v_{ry} + \sigma v_{rx})\,\mathrm{s}_{\phi_g} = \frac{1}{\sqrt{1+\sigma^2}}\left[\left(1+\sigma^2\right)v_{rx} + \sigma v_{ry}\right].$$

Therefore, by the definition (23), we obtain the front wheel longitudinal slip ratio

$$\lambda_{fs} = 1 - \frac{r\omega_f}{v_{fx_w}} = 1 - \frac{r\sqrt{1+\sigma^2}}{(1+\sigma^2)v_{rx} + \sigma v_{ry}}\omega_f. \tag{28}$$

3.2 Modeling of frictional forces

Modeling of the frictional forces between the tire and the road surface is complex. Here we focus on modeling of the longitudinal force F_x and lateral force F_y because of their importance in motorcycle dynamics and control.

The tire/road frictional forces depend on many factors, such as slip and slip angles, vehicle velocity, normal load, and tire and road conditions, etc. It is widely accepted that the pseudo-static relationships, namely, the mathematical models of the longitudinal force F_x and slip λ, and the lateral force F_y and slip angle γ, are the most useful characteristics to capture the tire/road interaction. To capture tire/road friction characteristics, we propose to approximate the friction forces by a piecewise linear relationship shown in Fig. 4. Let $F(x)$ denote the frictional force as a function of independent variable x. The piecewise linear function $F(x)$ captures the property of the tire/road forces: when $0 \le x \le x_m$, $F(x) = kx$, where k is the stiffness coefficient, and when $x_m < x \le x_{\max}$, $F = \frac{(1-\alpha_x)F_m}{x_m - x_{\max}}(x - x_m) + F_m$, where $0 \le \alpha_x \le 1$ is a constant that denotes the fraction of the force at $x_{\max}$ of the maximum force F_m. We can write the force $F(x)$ as follows.

$$F(x) = k(a_1 + a_2 x), \tag{29}$$

where

$$a_1 = \begin{cases} 0 & 0 \le x \le x_m \\ \frac{(x_{\max}-x_m)x_m}{x_{\max}-x_m} & x_m < x \le x_{\max}, \end{cases} \quad a_2 = \begin{cases} 1 & 0 \le x \le x_m \\ \frac{-(1-\alpha_x)x_m}{x_{\max}-x_m} & x_m < x \le x_{\max}. \end{cases}$$

With the force model (29), we can write the longitudinal force as

$$F_x(\lambda_s) = k_\lambda\left[a_{1\lambda} + a_{2\lambda}\,\mathrm{sign}(\lambda_s)\lambda_s\right], \tag{30}$$

where the function $\text{sign}(x) = 1$ for $x \geq 0$ and -1 otherwise is used to capture both positive (braking) and negative (traction) forces for $F_x(\lambda_s)$. For the lateral force, due to the large camber angle of the motorcycle tires, we have

$$F_y(\lambda_{eq}) = k_\gamma \left[a_{1\gamma} + a_{2\gamma}\,\text{sign}(\lambda_{eq})\lambda_{eq}\right], \tag{31}$$

where we define the equivalent side slip ratio

$$\lambda_{eq} = \tan\gamma_{eq} = \tan\left(\gamma + \frac{k_\varphi}{k_\gamma}\varphi\right) \approx \lambda_\gamma + \frac{k_\varphi}{k_\gamma}\tan\varphi.$$

The values of the longitudinal, corning, and cambering coefficients, k_λ, k_γ, k_φ, depend on the normal load F_z. Due to the acceleration and deceleration, the normal load F_z is changing during motion. For the front and rear wheels, the normal loads F_{fz} and F_{rz} are obtained respectively as

$$F_{fz} = \frac{b}{l}mg - \frac{h}{l}m\dot{v}_{Gx},\ F_{rz} = \frac{l-b}{l}mg + \frac{h}{l}m\dot{v}_{Gx}, \tag{32}$$

where $\dot{v}_{Gx}$ is the longitudinal acceleration of the motorcycle at the mass center G. The relationship between $\dot{v}_{Gx}$ and the acceleration of point C_2 is obtained as

$$\dot{v}_{Gx} = \dot{v}_{rx} - v_{ry}\dot{\psi} - h\ddot{\psi}\,\text{s}_\varphi - b\dot{\psi}^2 - 2h\dot{\psi}\dot{\varphi}\,\text{c}_\varphi\,.$$

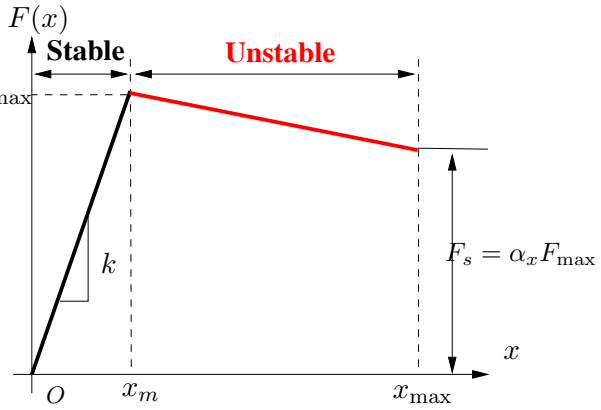

Figure 4: Linear approximation of the tire/road frictional force $F(x)$.

The calculation of the above relationship is given in Appendix B. In this work, we use the tire models in [37] to calculate the dependence of the stiffness coefficients with the normal load.

3.3 Combined tire and motorcycle dynamics models

We combine the motorcycle dynamics (17) and (21) with the tire dynamics. The controlled input variables are the front and rear wheel angular velocities, that is, ω_f and ω_r, respectively, and the steering angle ϕ. Note that the driving wheel is the rear wheel and we can only apply braking for the front wheel, namely, $F_{fx} \geq 0$. For the control system design, we consider the pseudo-static friction models (30) and (31), and therefore we write the longitudinal at the front and rear wheels as

$$F_{fx} = F_{1f} + F_{2f}\lambda_{fs},\ \ F_{rx} = F_{1r} + F_{2r}\lambda_{rs} \tag{33}$$

and lateral forces

$$F_{fy} = F_{3f} + F_{4f}\left(\lambda_{f\gamma} + \frac{k_{f\varphi}}{k_{f\gamma}}\tan\varphi_f\right),\ F_{ry} = F_{3r} + F_{4r}\left(\lambda_{r\gamma} + \frac{k_{r\varphi}}{k_{r\gamma}}\tan\varphi\right), \tag{34}$$

where $F_{1i} = k_{i\lambda}a_{1i\lambda}$, $F_{2i} = k_{i\lambda}a_{2i\lambda}\,\text{sign}(\lambda_{is})$, $F_{1i} = k_{i\lambda}a_{1i\lambda}$, $F_{2i} = k_{i\lambda}a_{2i\lambda}\,\text{sign}(\lambda_{is})$, $i = f, r$, and $a_{ji\lambda}$, $a_{ji\gamma}$, $j = 1, 2$, are the longitudinal and lateral force model parameters defined in (29), respectively.

Plugging (33) and (34) into (21) and using the relationship (27), we obtain

$$\mathbf{M}(\boldsymbol{q}, \sigma)\ddot{\boldsymbol{q}} = \mathbf{K}(\dot{\boldsymbol{q}}, \boldsymbol{q}, \sigma) + \mathbf{B}\boldsymbol{u}, \tag{35}$$

where input $\boldsymbol{u} := \begin{bmatrix}\omega_\sigma & \boldsymbol{u}_\lambda^T\end{bmatrix}^T$, $\boldsymbol{u}_\lambda = \begin{bmatrix}\lambda_{fs} & \lambda_{rs}\end{bmatrix}^T$, matrix

$$\mathbf{K} = \begin{bmatrix}K_1 \\ \hdashline K_2\end{bmatrix} = \left[\begin{array}{c} (K_m)_1 \\ \hdashline (K_m)_2 - \dfrac{F_{1f}}{m\sqrt{1+\sigma^2}} - \dfrac{\sigma}{m\sqrt{1+\sigma^2}}F_{34} + \dfrac{F_{1r}}{m} \\ (K_m)_3 - \dfrac{\sigma F_{1f}}{m\sqrt{1+\sigma^2}} + \dfrac{1}{m\sqrt{1+\sigma^2}}F_{34} - \dfrac{F_{ry}}{m}\end{array}\right], \tag{36}$$

$(K_m)_i$ is the ith row of matrix $\mathbf{K}$, $F_{34} = F_{3f} + F_{4f}\left(\lambda_{f\gamma} + \frac{k_{f\varphi}}{k_{f\gamma}}(2\sigma - \lambda_{r\gamma})\right)$, and

$$\mathbf{B} = \begin{bmatrix} B_{11} & B_{12} \\ \hdashline B_{21} & B_{22} \end{bmatrix} = \left[\begin{array}{c:cc} -\dfrac{bh}{l}\,\mathrm{c}_\varphi\, v_{rx} & 0 & 0 \\ \hdashline B_\omega + \dfrac{r\sigma F_{4f}\tan\xi\,\mathrm{c}_\varphi^2\,k_{f\varphi}}{m v_{rx} k_{f\gamma}\sqrt{1+\sigma^2}} & -\dfrac{F_{2f}}{m\sqrt{1+\sigma^2}} & \dfrac{F_{2r}}{m} \\ -\dfrac{bv_{rx}}{l} - \dfrac{rF_{4f}\tan\xi\,\mathrm{c}_\varphi^2\,k_{f\varphi}}{m v_{rx} k_{f\gamma}\sqrt{1+\sigma^2}} & -\dfrac{\sigma F_{2f}}{m\sqrt{1+\sigma^2}} & 0 \end{array}\right]. \tag{37}$$

In the next section, we will develop a trajectory tracking and balancing control for dynamics (35).

4 Trajectory Tracking Control Systems Design

4.1 External/Internal convertible dynamical systems

We now consider to put the system into the form of an external/Internal convertible (EIC) dynamical systems. The EIC form of a nonlinear dynamical system can be viewed as a special case of the normal form.

Definition 1 ([9]) *A single-input, single-output, $n(=m+p)$-dimensional time-invariant nonlinear control system is called in an* external/internal convertible form *if the system is of the form*

$$\Sigma(u)\begin{cases} \dot{x}_i = x_{i+1}, & i = 1, \cdots, m-1, \\ \dot{x}_m = u, & \\ \dot{\alpha}_i = \alpha_{i+1}, & i = 1, \cdots, p-1, \\ \dot{\alpha}_p = f(x,\alpha) + g(x,\alpha)u, & \\ y = x_1, & \end{cases} \tag{38}$$

with input $u \in \mathbb{R}$, output $y \in \mathbb{R}$, state variables (x, α), with $x := (x_1, \cdots, x_m) \in \mathbb{R}^m$ and $\alpha := (\alpha_1, \cdots \alpha_p) \in \mathbb{R}^p$. The coordinates (x, α) are assumed to be defined on the open ball $\mathbf{B}_r \subset \mathbb{R}^n$ about the origin. The origin is assumed to be an equilibrium of the system, namely, $f(0,0) = 0$. The functions $f(x,\alpha)$ and $g(x,\alpha)$ are C^n in their arguments, and $g(x,\alpha) \neq 0$ for all $(x,\alpha) \in \mathbf{B}_r$. Moreover, we refer to the external subsystem *of $\Sigma(u)$ as*

$$\Sigma_{\mathrm{ext}}(u)\begin{cases} \dot{x}_i = x_{i+1}, & i = 1, \cdots, m-1, \\ \dot{x}_m = u, & \end{cases} \tag{39}$$

and the internal subsystem *of $\Sigma(u)$ as*

$$\Sigma_{\mathrm{int}}(u)\begin{cases} \dot{\alpha}_i = \alpha_{i+1}, & i = 1, \cdots, p-1, \\ \dot{\alpha}_p = f(x,\alpha) + g(x,\alpha)u. & \end{cases} \tag{40}$$

Fig. 5 shows the structure of an EIC system. An EIC system is *convertible* because under a simple state-dependent input and an output transformation, the internal system is converted to an external system, and the external system is converted to an internal system (*dual* structure). To see such a property, let

$$u = g(x,\alpha)^{-1}\left[v - f(x,\alpha)\right] \tag{41}$$

define a state-dependent input transformation, $u \mapsto v$. Define $\xi = \alpha^1$ as the *dual output*. Apply transformation (41) to the EIC system (38) and the resulting system is referred to the *dual* of $\Sigma(u)$.

$$\Sigma_d(v)\begin{cases} \dot{x}_i = x_{i+1}, & i = 1, \cdots, m-1, \\ \dot{x}_m = -g(x,\alpha)^{-1}f(x,\alpha) + g(x,\alpha)^{-1}v, & \\ \dot{\alpha}_i = \alpha_{i+1}, & i = 1, \cdots, p-1, \\ \dot{\alpha}_p = v, & \\ \xi = \alpha_1. & \end{cases} \tag{42}$$

Thus the use of input transformation (41) and the output assignment $\xi = \alpha_1$ converts the internal dynamics of $\Sigma(u)$ to the external dynamics of $\Sigma_d(v)$, and the external dynamics of $\Sigma(u)$ to the internal dynamics of $\Sigma_d(v)$.

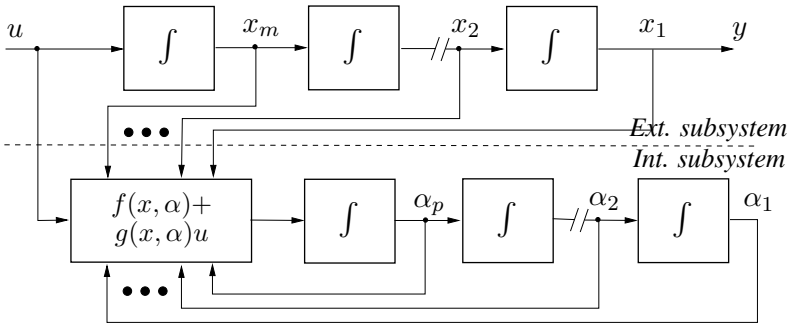

Figure 5: An external/internal convertible system.

Since the EIC form is a special normal form of nonlinear dynamical systems, we can apply the input-output linearization method [25, 38] to convert (35) into an EIC form. Let $B_{22} \in \mathbb{R}^{2\times 2}$, $B_{22} \in \mathbb{R}^{2\times 2}$, and $K_2 \in \mathbb{R}^2$ denote the block elements of matrices $\mathbf{M}$, $\mathbf{B}$, and $\mathbf{K}$, given by (22), (37), and (36), respectively. Using the input transformation

$$\boldsymbol{u}_\lambda = B_{22}^{-1} M_{22} \left[M_{22}^{-1} \left(M_{21} \ddot{\varphi} - K_2 - B_{21} \omega_\sigma \right) + \boldsymbol{u}_a \right], \tag{43}$$

Eq. (35) becomes

$$\begin{cases} M_{11} \ddot{\varphi} = K_1 - M_{12} \boldsymbol{u}_a + B_{11} \omega_\sigma \,, \\ \begin{bmatrix} \dot{v}_{rx} \\ \dot{v}_{ry} \end{bmatrix} = \begin{bmatrix} a_{rx} \\ a_{ry} \end{bmatrix} =: \boldsymbol{u}_a, \end{cases} \tag{44}$$

where $\boldsymbol{u}_a$ is the controlled acceleration of point C_2 in the xyz coordinate system. We also define the controlled jerk of point C_2 and yaw acceleration as

$$\boldsymbol{u}_j := \begin{bmatrix} u_{rx} \\ u_{ry} \\ u_\psi \end{bmatrix} = \begin{bmatrix} \dot{a}_{rx} \\ \dot{a}_{ry} \\ \ddot{\psi} \end{bmatrix} = \begin{bmatrix} \dot{\boldsymbol{u}}_a \\ \frac{v_{rx}\omega_\sigma + \sigma a_{rx}}{l} \end{bmatrix}, \tag{45}$$

where we use kinematics $l\dot{\psi} = \sigma v_{rx}$ in the calculation. Let (X, Y) denote the coordinates of the contact point C_2 and then we have

$$\begin{bmatrix} v_X \\ v_Y \end{bmatrix} = \begin{bmatrix} \dot{X} \\ \dot{Y} \end{bmatrix} = \begin{bmatrix} \mathrm{c}_\psi & -\mathrm{s}_\psi \\ \mathrm{s}_\psi & \mathrm{c}_\psi \end{bmatrix} \begin{bmatrix} v_{rx} \\ v_{ry} \end{bmatrix}.$$

Differentiating the above equation twice (dynamic extension), we obtain

$$\begin{bmatrix} \ddot{v}_X \\ \ddot{v}_Y \end{bmatrix} = \mathbf{U} + \boldsymbol{u}_J, \tag{46}$$

where

$$\mathbf{U} = \begin{bmatrix} -2\dot{v}_{rx}\,\mathrm{s}_\psi - 2\dot{v}_{ry}\,\mathrm{c}_\psi - v_{rx}\dot{\psi}\,\mathrm{c}_\psi + v_{ry}\dot{\psi}\,\mathrm{s}_\psi \\ 2\dot{v}_{rx}\,\mathrm{c}_\psi - 2\dot{v}_{ry}\,\mathrm{s}_\psi - v_{rx}\dot{\psi}\,\mathrm{s}_\psi - v_{ry}\dot{\psi}\,\mathrm{c}_\psi \end{bmatrix} \dot{\psi}, \; \boldsymbol{u}_J := \begin{bmatrix} \mathrm{c}_\psi & -\mathrm{s}_\psi \\ \mathrm{s}_\psi & \mathrm{c}_\psi \end{bmatrix} \begin{bmatrix} u_{rx} \\ u_{ry} \end{bmatrix} + \begin{bmatrix} -v_{rx}\,\mathrm{s}_\psi - v_{ry}\,\mathrm{c}_\psi \\ v_{rx}\,\mathrm{c}_\psi - v_{ry}\,\mathrm{s}_\psi \end{bmatrix} u_\psi. \tag{47}$$

We define the new inputs u_X and u_Y such that

$$\boldsymbol{u}_J = -\mathbf{U} + \begin{bmatrix} u_X \\ u_Y \end{bmatrix} \tag{48}$$

and then the motorcycle dynamics (44) are in the EIC form as

$$\Sigma_{\text{ext}}: \left\{ \begin{bmatrix} \ddot{v}_X \\ \ddot{v}_Y \end{bmatrix} = \begin{bmatrix} u_X \\ u_Y \end{bmatrix}, \right. \tag{49a}$$

$$\Sigma_{\text{int}}: \ddot{\varphi} = \frac{g}{h}\left(\mathrm{s}_\varphi + \frac{bl_t\,\mathrm{c}_\xi\,\dot{\psi}}{hv_{rx}}\,\mathrm{c}_\varphi\right) - \frac{1}{h}\Big(1 - \frac{h\dot{\psi}}{v_{rx}}\,\mathrm{s}_\varphi\Big)\dot{\psi}v_{rx}\,\mathrm{c}_\varphi - \frac{1}{h}\,\mathrm{c}_\varphi\,u_{\psi y}, \tag{49b}$$

where

$$u_{\psi y} := bu_\psi + a_{ry}. \tag{50}$$

Remark 3 *When the motorcycle runs along a straight-line, $\sigma = 0$ and matrix B_{22} becomes singular and we cannot use input transformation (43). In this case, we calculate the total braking force from the second equation of the motions and split two the front and rear wheels in a way not producing any net moments around mass center G. A similar approach is discussed in [39]. If the resultant total force is traction, then it must be produced by the rear wheel.*

4.2 Trajectory tracking control

4.2.1 Control system overview

The trajectory control system then guides the motorcycle to follow the desired trajectory $\mathcal{T}$: $(X_d(t), Y_d(t))$ while keeping the platform balanced and stable. We here employ and extend the control design approach in [9]. Fig. 6 illustrates such a control scheme. The trajectory control design consists of two steps. The first step to design a tracking control $\mathbf{u}_{\text{ext}}$ of the external subsystem Σ_{ext} for the desired trajectory $\mathcal{T}$. The second step is to design a balancing controller for the internal subsystem Σ_{int} around the internal equilibrium manifold, denoted as $\mathcal{E}(t)$. The internal equilibrium manifold $\mathcal{E}(t)$ is an embedded sub-manifold in the state space and dependent on the external control $\mathbf{u}_{\text{ext}}$ and the external subsystem. Estimations of internal equilibrium and its derivatives are obtained by a dynamic inversion technique [9]. The final control system is a combination of external and internal design and is casual.

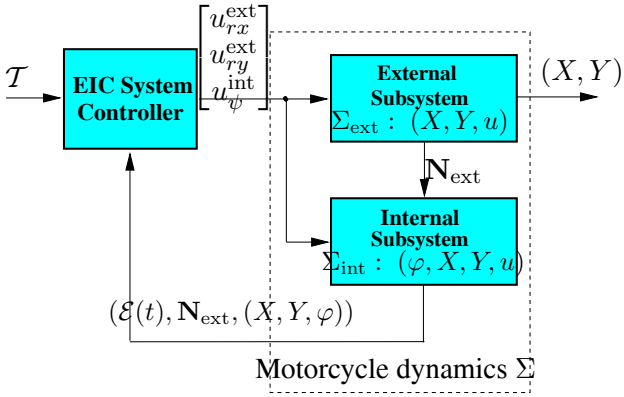

Figure 6: EIC-based approximate output tracking control of the autonomous motorcycle dynamics.

4.2.2 Approximate tracking control

We assume that the desired trajectory $\mathcal{T}: (X_d(t), Y_d(t))$ is at least C^4, namely, differentiable at least to fourth order [5]. This is feasible since the motion planning algorithm can usually generate a set of piecewise circular curves (C^∞) for $\mathcal{T}$ [40].

We design a controller $\mathbf{u}_{\text{ext}}$ to track the desired trajectory $(X_d(t), Y_d(t))$ for the external subsystem Σ_{ext} (49a) disregarding, for the moment, the evolution of the internal subsystem Σ_{int} (49b).

$$\boldsymbol{u}^{\text{ext}} := \begin{bmatrix} u_X^{\text{ext}} \\ u_Y^{\text{ext}} \end{bmatrix} = \begin{bmatrix} X_d^{(3)} \\ Y_d^{(3)} \end{bmatrix} - \sum_{i=1}^{3} b_i \begin{bmatrix} X^{(i-1)} - X_d^{(i-1)} \\ Y^{(i-1)} - Y_d^{(i-1)} \end{bmatrix}, \tag{51}$$

[5] For the external subsystem control, we only need $\mathcal{T}$ to be C^3. The requirement for C^4 is due to the estimation of the internal (roll angle) equilibrium and its derivatives by a dynamic inversion technique.

where the constants b_i, $i = 1, 2, 3$, are chosen such that the polynomial equation $s^3 + b_3 s^2 + b_2 s + b_1 = 0$ is Hurwitz. Under such a control, we define a nominal external vector field $\mathbf{N}_{\rm ext}$ as

$$\mathbf{N}_{\rm ext} := \begin{bmatrix} \dot{X}(t) \\ \ddot{X}(t) \\ X_d^{(3)} - \sum_{i=1}^3 b_i \left(X^{(i-1)} - X_d^{(i-1)} \right) \\ \dot{Y}(t) \\ \ddot{Y}(t) \\ Y_d^{(3)} - \sum_{i=1}^3 b_i \left(Y^{(i-1)} - Y_d^{(i-1)} \right) \end{bmatrix}, \tag{52}$$

By external control (51) and the input transformation (48), we find the input $\boldsymbol{u}_J^{\rm ext} = -\mathbf{U} + \boldsymbol{u}^{\rm ext}$. From (47), we obtain $\boldsymbol{u}_j^{\rm ext}$ as

$$\begin{bmatrix} u_{rx} \\ u_{ry} \end{bmatrix} + \begin{bmatrix} -v_{ry} \\ v_{rx} \end{bmatrix} u_\psi = \begin{bmatrix} \mathrm{c}_\psi & \mathrm{s}_\psi \\ -\mathrm{s}_\psi & \mathrm{c}_\psi \end{bmatrix} \boldsymbol{u}_J. \tag{53}$$

Note that $\boldsymbol{u}_J \in \mathbb{R}^2$ and $\boldsymbol{u}_j \in \mathbb{R}^3$ and the above equation is underdetermined. There are many options to determine $\boldsymbol{u}_j$ from (53). Here we propose to choose $u_\psi = \ddot{\psi} = 0$ because such a choice significantly reduces the complexity of the control design as shown in the following.

$$\boldsymbol{u}_j^{\rm ext} = \begin{bmatrix} u_{rx}^{\rm ext} \\ u_{ry}^{\rm ext} \\ u_\psi^{\rm ext} \end{bmatrix} = \begin{bmatrix} \boldsymbol{R}(\psi) \boldsymbol{u}_J^{\rm ext} \\ 0 \end{bmatrix} = \begin{bmatrix} \boldsymbol{R}(\psi) \left(-\mathbf{U} + \boldsymbol{u}^{\rm ext} \right) \\ 0 \end{bmatrix}. \tag{54}$$

Next, we consider the internal (roll angle) equilibrium, denoted as φ_e, by substituting $u_\psi^{\rm ext}$ and $u_{ry}^{\rm ext}$ above into the internal subsystem dynamics (49b). We define the implicit function F_φ of φ as

$$F_\varphi := g \left(\tan\varphi + \frac{b l_t \dot{\psi}\, \mathrm{c}_\xi}{h v_{rx}} \right) - \left(1 - \frac{h \dot{\psi}\, \mathrm{s}_\varphi}{v_{rx}} \right) \dot{\psi} v_{rx} - u_{\psi y}^{\rm ext}, \tag{55}$$

$u_{\psi y}^{\rm ext} = b u_\psi^{\rm ext} + a_{ry} = a_{ry}$, and thus the roll angle equilibrium $\varphi_e := \varphi_e(\dot{\psi}, v_{rx}, \boldsymbol{u}_j^{\rm ext})$ is a solution of the algebraic equation $F_{\varphi_e} = 0$. We define an internal (roll angle) equilibrium manifold $\mathcal{E}(t)$ as

$$\mathcal{E}(t) = \left\{ \left(X^{(0,2)}, Y^{(0,2)}, \varphi^{(0,1)} \right) \mid \varphi = \varphi_e,\ \dot{\varphi} = 0 \right\}. \tag{56}$$

The internal equilibrium manifold $\mathcal{E}(t)$ can be viewed as a time-dependent graph over the 6-dimensional (X, Y)-subspace in $\mathbb{R}^6$ of the external subsystem (49a) that is evolved with the external nominal vector field $\mathbf{N}_{\rm ext}$ (52) under the external subsystem control $\boldsymbol{u}^{\rm ext}$.

For the motorcycle balance systems, we like to control the roll angle φ around $\mathcal{E}(t)$ while the external subsystem is tracking $\mathcal{T}$ under the control of $\boldsymbol{u}^{\rm ext}$. Note that $\dot{\varphi}_e \neq 0$ and $\ddot{\varphi}_e \neq 0$ in general and here we approximate the derivatives $\dot{\varphi}_e$ and $\ddot{\varphi}_e$ by using directional derivatives [25, 38] along the vector field $\mathbf{N}_{\rm ext}$ due to their dependence on the external subsystems and $\boldsymbol{u}^{\rm ext}$. We define the directional derivative (or Lie derivative) as $\bar{L}_{\mathbf{N}_{\rm ext}} \varphi_e := L_{\mathbf{N}_{\rm ext}} \varphi_e + \frac{\partial \varphi_e}{\partial t}$ and $\bar{L}^2_{\mathbf{N}_{\rm ext}} \varphi_e := \bar{L}_{\mathbf{N}_{\rm ext}} \bar{L}_{\mathbf{N}_{\rm ext}} \varphi_e$. With the above approximations for $\dot{\varphi}_e$ and $\ddot{\varphi}_e$, the stabilizing control of the internal subsystem $\Sigma_{\rm int}$ (49b) around $\mathcal{E}(t)$ is then given by the following feedback linearization

$$u_{\psi y}^{\rm int} = \left(\frac{\mathrm{c}_\varphi}{h} \right)^{-1} \left[\frac{g}{h} \left(\mathrm{s}_\varphi + \frac{b l_t\, \mathrm{c}_\xi\, \dot{\psi}}{h v_{rx}}\, \mathrm{c}_\varphi \right) - \frac{1}{h} \left(1 - \frac{h \dot{\psi}}{v_{rx}}\, \mathrm{s}_\varphi \right) \dot{\psi} v_{rx}\, \mathrm{c}_\varphi - v_{\psi y} \right], \tag{57a}$$

$$v_{\psi y} = \bar{L}^2_{\mathbf{N}_{\rm ext}} \varphi_e - \sum_{i=1}^{2} a_i (\varphi^{(i-1)} - \bar{L}^{i-1}_{\mathbf{N}_{\rm ext}} \varphi_e). \tag{57b}$$

where constants a_1 and a_2 are chosen such that the polynomial equation $s^2+a_2s+a_1=0$ is Hurwitz. Therefore, the internal control is obtained from (50) as

$$u_\psi^{\rm int} = \frac{1}{b}\left(u_{\psi y}^{\rm int} - a_{ry}\right) \tag{58}$$

The *final* control system design of the motorcycle balance system (46) combines the above development in (58) and (54) as

$$\boldsymbol{u}_j = \begin{bmatrix} u_{rx}^{\rm ext} \\ u_{ry}^{\rm ext} \\ u_\psi^{\rm int} \end{bmatrix} \tag{59}$$

It is noted that the coupling between the external- and internal-subsystem control designs is through the introduction of the internal equilibrium manifold $\mathcal{E}(t)$. By defining $\mathcal{E}(t)$, we approximately decouple the external and internal subsystems due to the EIC dual structural properties of the motorcycle system.

We define $\boldsymbol{\vartheta}(t) = [X(t)\ v_X(t)\ \dot{v}_X(t)\ Y(t)\ v_Y(t)\ \dot{v}_Y(t)]^T$ as the state variables of the external subsystem and $\boldsymbol{\varrho}(t) = [\varphi(t)\ \dot{\varphi}(t)]^T$ as the state variables of the internal subsystem. We also define the output $\boldsymbol{\zeta}(t) = [X(t)\ Y(t)]^T$ and desired output $\boldsymbol{\zeta}_d(t) = [X_d(t)\ Y_d(t)]^T$. We assume that the desired trajectory $\boldsymbol{\zeta}_d(t)$ and its derivatives (up to the fourth order) are bounded by a positive number $\epsilon > 0$, namely, $\boldsymbol{\zeta}_d(t) \in \mathbf{B}_\epsilon^{(4)} := \{\boldsymbol{x}(t) \mid \|\boldsymbol{x}^{(0,4)}(t)\|_\infty < \epsilon\}$, where $\|\boldsymbol{x}^{(0,n)}(t)\|_\infty := \sup_{t\geq 0}\|\boldsymbol{x}^{(0,n)}(t)\|_\infty$. We also define the tracking errors $e_i^\vartheta = \vartheta_i - X_d^{(i-1)}$, $e_{i+3}^\vartheta = \vartheta_{i+3} - Y_d^{(i-1)}$, $i=1,2,3$, $e_j^\varphi = \varphi^{(j)} - \varphi_e^{(j)}$, $j=0,1$, and $\boldsymbol{e} := [e_1^\vartheta,\ \cdots,\ e_6^\vartheta,\ e_1^\varphi,\ e_2^\varphi]^T$. We also define the perturbation error p_φ ($= O(\|\boldsymbol{\zeta}_d^{(0,4)}(t)\|, \|\boldsymbol{e}\|)$ as the approximation errors by using the directional derivatives for $\dot{\varphi}_e$ and $\ddot{\varphi}_e$ in the internal subsystem control design (57b), namely,

$$p_\varphi = \bar{L}_{\mathbf{N}_{\rm ext}}^2 \varphi_e - \ddot{\varphi}_e + \sum_{i=1}^{2} a_i(\varphi_e^{(i-1)} - \bar{L}_{\mathbf{N}_{\rm ext}}^{i-1}\varphi_e).$$

We similarly define another two perturbation errors p_X ($= O(\|\boldsymbol{\zeta}_d^{(0,4)}(t)\|, \|\boldsymbol{e}\|)$ and p_Y ($= O(\|\boldsymbol{\zeta}_d^{(0,4)}(t)\|, \|\boldsymbol{e}\|)$ due to the resulting errors in the external subsystem state $\boldsymbol{\vartheta}(t)$ using the internal subsystem control $u_{\psi y}^{\rm int}$ in the external subsystem (59). An explicit formulation for p_X and p_Y can be similarly found by the dual structure of EIC system [9]. We consider the perturbation vector for the error dynamics of $\Sigma(u)$ (48) under control (59) as

$$p(\boldsymbol{\zeta}_d^{(0,4)}(t), \boldsymbol{e}) = [0,\ 0,\ p_X,\ 0,\ 0,\ p_Y,\ 0,\ p_\varphi]^T.$$

We assume an affine perturbation for $p(y_d^{(0,4)}(t), e)$, namely, there exist constants $k_1 > 0$ and $k_2 > 0$ such that $\|p(\boldsymbol{\zeta}_d^{(0,5)}(t), \boldsymbol{e})\|_\infty \leq k_1\epsilon + k_2\|\boldsymbol{e}\|_\infty$.

We only state the convergence properties of the approximate tracking control design in this section. The proof of these properties follows directly from Proposition 6.7.4 and Theorem 6.7.6 in [9] and we omit here.

Theorem 1 *For the balance system (48), assuming that the desired trajectory $\boldsymbol{\zeta}_d(t) \in \mathbf{B}_\epsilon^{(4)}$ for some $\epsilon > 0$ and if the affine perturbation constant $k_2 > 0$ is a sufficiently small real number, then there exists a $t_1 > 0$, and a class-$\mathcal{K}$ function $r(\epsilon)$ such that for all $(\boldsymbol{e}^\vartheta(0), \boldsymbol{e}^\varphi(0)) \in \mathbf{B}_{r(\epsilon)}$, $(\boldsymbol{e}^\vartheta(t), \boldsymbol{e}^\varphi(t))$ converges to zero exponentially until $(\boldsymbol{e}^\vartheta(t), \boldsymbol{e}^\varphi(t))$ enters $\mathbf{B}_{r(\epsilon)}$. Once $(\boldsymbol{e}^\vartheta(t), \boldsymbol{e}^\varphi(t))$ enters $\mathbf{B}_{r(\epsilon)}$, it will stay in $\mathbf{B}_{r(\epsilon)}$ thereafter.*

4.2.3 Estimation of the internal equilibrium

A dynamic inversion technique approach in [9] is used to estimate the internal equilibrium state φ_e in (57b). To illustrate the dynamic inversion technique, we differentiate $F_\varphi = 0$ with time, and using the fact that $u_\psi^{\rm ext} = \ddot{\psi} = 0$ we obtain

$$\dot{\varphi}_e = \frac{1}{g\sec^2\varphi_e + h\dot{\psi}\,\mathrm{c}_{\varphi_e}}\left(\frac{gbl_t\,\mathrm{c}_\xi\,\dot{\psi}\dot{v}_{rx}}{hv_{rx}^2} + \dot{\psi}\dot{v}_{rx} + u_{ry}^{\rm ext}\right) =: E(\varphi_e, \dot{\psi}, v_{rx}, \dot{v}_{rx}, u_{ry}^{\rm ext}). \tag{60}$$

A dynamic inverter for an estimate $\hat{\varphi}_e$ of the internal equilibrium φ_e is designed as

$$\dot{\hat{\varphi}}_e = -\beta F_{\hat{\varphi}} + E(\hat{\varphi}_e, \dot{\psi}, v_{rx}, \dot{v}_{rx}, u_{ry}^{\text{ext}}), \tag{61}$$

where $F_{\hat{\varphi}_e}$ is given by (55) and $\beta > 0$ is the inverter gain. The proof of the exponential convergence of the estimation (61) follows directly from the development of the dynamic inversion technique in [9].

The estimate of the directional derivative $\bar{L}_{\mathbf{N}_{\text{ext}}}\varphi_e$ in (57b) is obtained by (61), namely, $\bar{L}_{\mathbf{N}_{\text{ext}}}\varphi_e = E(\varphi_e, \dot{\psi}, v_{rx}, \dot{v}_{rx}, u_{ry}^{\text{ext}})$. The estimate of $\bar{L}^2_{\mathbf{N}_{\text{ext}}}\varphi_e$ is obtained by directly taking one more directional derivative of $\bar{L}_{\mathbf{N}_{\text{ext}}}\varphi_e$ along $\mathbf{N}_{\text{ext}}$. For brevity, we give the derivation in Appendix C. We also list the calculation of $\bar{L}_{\mathbf{N}_{\text{ext}}}u_{rx}^{\text{ext}}$ and $\bar{L}_{\mathbf{N}_{\text{ext}}}u_{ry}^{\text{ext}}$ in Appendix C. Such calculations are needed for computing $\bar{L}^2_{\mathbf{N}_{\text{ext}}}\varphi_e$. The approximation errors in estimating φ_e (by $\hat{\varphi}_e$) and its directional derivatives $\bar{L}_{\mathbf{N}_{\text{ext}}}\varphi_e$ and $\bar{L}^2_{\mathbf{N}_{\text{ext}}}\varphi_e$ (by $\bar{L}_{\mathbf{N}_{\text{ext}}}\hat{\varphi}_e$ and $\bar{L}^2_{\mathbf{N}_{\text{ext}}}\hat{\varphi}_e$, respectively) can be considered as additional terms in the perturbation $p(\boldsymbol{\zeta}_d^{(0,4)}(t), \boldsymbol{e})$. Therefore, the stability results of the approximate control design in the previous section are still held.

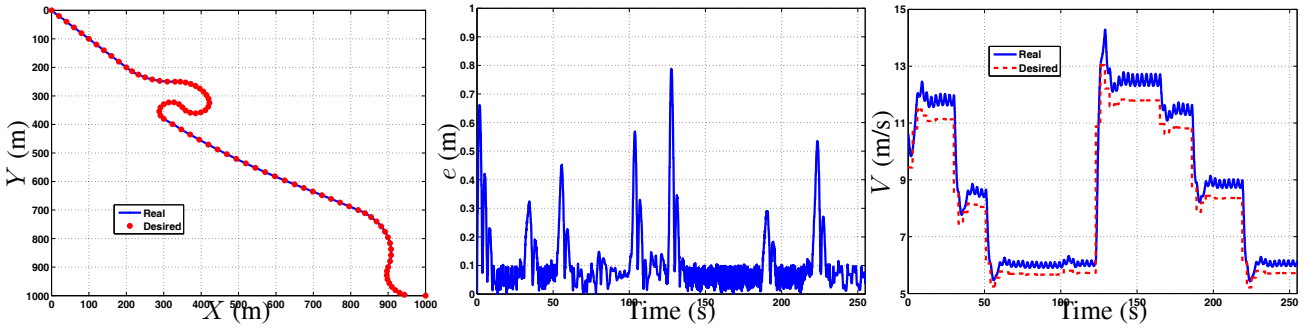

(a) (b) (c)

Figure 7: A general trajectory tracking. (a) Trajectory positions. (b) Tracking position error. (c) Rear wheel contact point velocity magnitude.

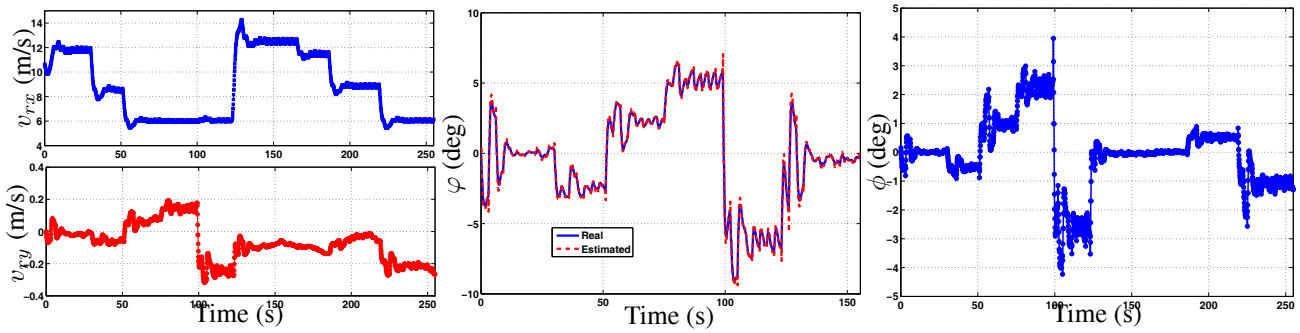

(a) (b) (c)

Figure 8: Roll angle and steering angle of the general trajectory tracking. (a) Rear wheel contact point body-frame velocities v_{rx} and v_{ry}. (b) Roll angle φ. (b) Steering angle ϕ.

Remark 4 *Although the above control system design is similar to those in [9], the final form is much simpler because we have chosen* $u_{\psi}^{\text{ext}} = 0$ *in (54). We have such a flexibility by (53) to determine* $\boldsymbol{u}_j$ *because we have three control input variables now while in [9] only the rear wheel driving torque and the steering angle are controlled. Because of this difference, we only require the trajectory* $\mathcal{T}$ *is at least* C^4 *rather than* C^5 *as the requirement of the controller in [9]. Using optimization techniques by considering the input constraints for determining* $\boldsymbol{u}_j$ *by (53) is an extension of the control design and currently ongoing research.*

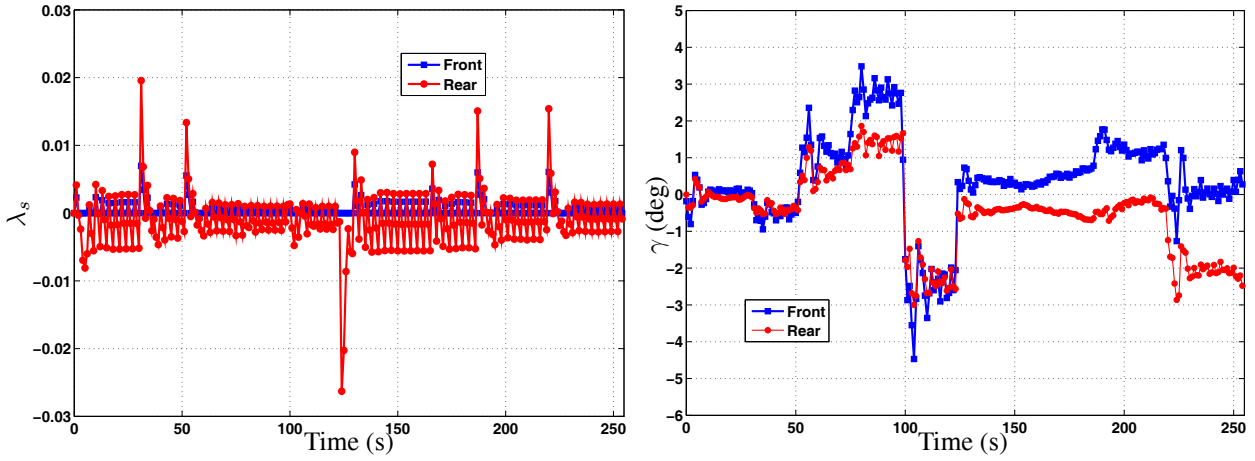

Figure 9: Longitudinal slips and slip angles at the front and rear wheels. (a) Slip ratio λ_{fs} and λ_{rs}. (b) Slip angles γ_f and γ_r.

Table 1: Motorcycle parameters

m (kg)	b (m)	l (m)	l_t (m)	h (m)	ξ (deg)	r (m)	λ_{sm}	$\lambda_{\gamma m}$ (deg)	μ_m	k_λ (N)	k_φ (N/rad)	k_γ (N)
274.2	0.81	1.37	0.15	0.62	26.1	0.3	0.1	6	3	41504	23968	1227

4.3 Simulation Results

In this section, we demonstrate the control systems design through two numerical examples. The first example is taken from [16] for showing a general motorcycle trajectory and the second example to illustrate an aggressive maneuvers with a large side slip angles.

We use a racing motorcycle prototype in [37, 41] as the controlled motorcycle in our simulation. The motorcycle parameters are listed in Table 1. We use the tire 160/70 in [37] for the racing motorcycle since the testing data are available. The tire stiffness coefficients listed in Table 1 are calculated under the nominal load $F_z = 1600$ N.

Fig. 7 shows the trajectory tracking performance of a general trajectory. The position errors under the control system in Fig. 7(b) are within 1 meter with the center line of the track throughout the entire course. The desired velocity in Fig. 7(c) is determined by the curvature of the trajectory. In Fig. 8, we have shown the roll angle φ, the body-frame velocities v_{rx} and v_{ry} of rear wheel contact point C_2, and steering angle ϕ. From Fig. 8(a) we clearly see that the lateral velocity v_{ry} is quite small most time because the motorcycle is running along a straight-line in most time. At turning locations, the longitudinal velocity is reduced and the lateral velocity increases. The roll angle and steering angle are small for such a small-curvature trajectory.

Fig. 9 shows the longitudinal slips and side slip angles of the front and rear wheels. Again, it is clear that the slip values at both wheels are small. The front wheel only brakes and the rear wheel generates traction or braking forces. For example, when the motorcycle accelerates around 120 s, the rear wheel slip has a large negative spike to produce the traction force. When the vehicle needs to reduce velocity, both wheels brake with a set of large positive slip spikes shown in Fig. 9(a). The side slip angles shown in Fig. 9(b) clearly illustrate that at large-curvature locations, the side slip angles are large to produce the lateral forces to turn the motorcycle. Typically, the rear side slip angles are small and close to zero.

The second example shows that the motorcycle runs under a more aggressive maneuver. The desired trajectory is "8"-shape with circular radius of 25 meters; see Fig. 10(a). In Fig. 10(a), the motorcycle starts from the origin and moves along the direction indicated by the arrows in the figure. The desired velocity of the motorcycle moving along the "8"-shape trajectory is designed to be varying significantly as shown in Fig. 10(c). Comparing

with the previous example, the tracking errors of the "8"-shape trajectory are much larger; see Fig. 10(b). This is mainly due to the quick change of the desired velocity profile.

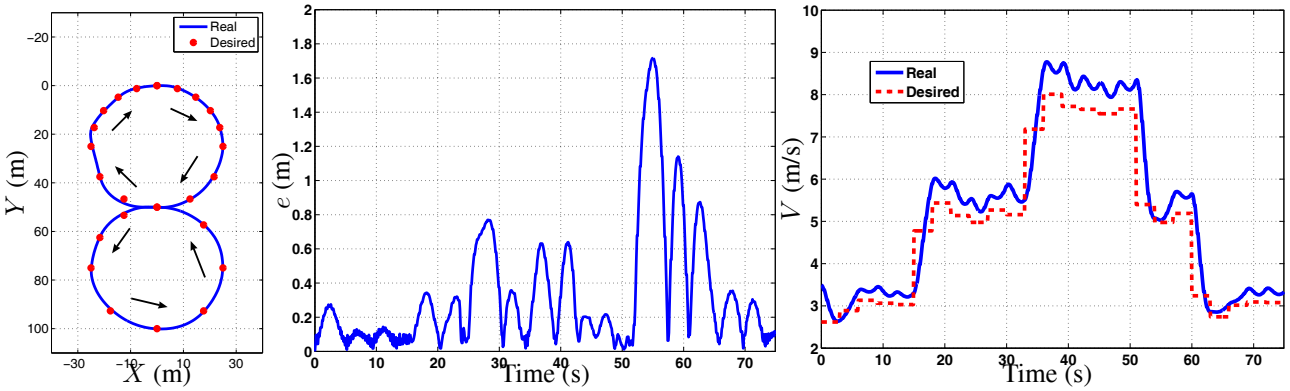

(a) (b) (c)

Figure 10: An "8"-shape trajectory tracking. (a) Trajectory positions. (b) Tracking position error. (c) Rear wheel contact point velocity magnitude.

Fig. 11 shows the body-frame velocity, roll angle, and steering angle for the "8"-shape trajectory. We clearly see the change of the lateral velocity during each circle of the "8"-shape trajectory. The lateral velocity magnitude is large due to the smaller turning radius. The maximum roll angle is around 15 deg and that is much larger than that of the previous example. The steering angle is large as well to make the motorcycle turn in a tighter and small circle. The oscillations in both roll angle (Fig. 11(b)) and steering angle (Fig. 11(c)) are probably due to the variations in the desired velocity.

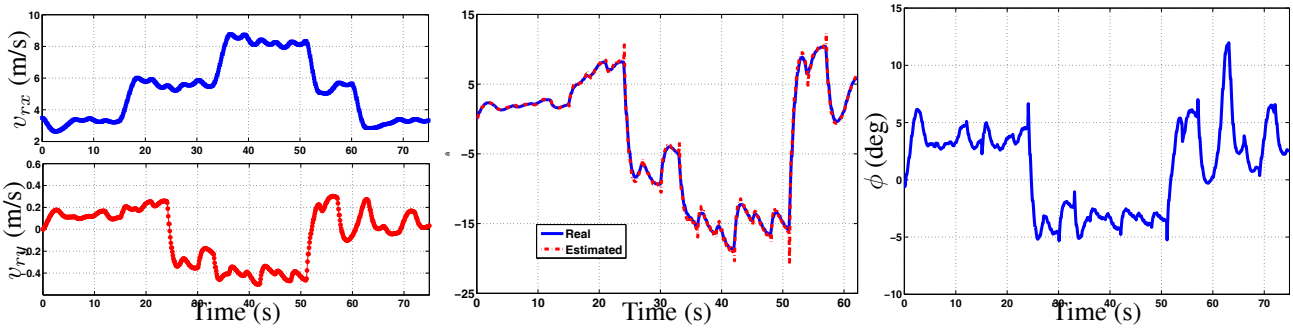

(a) (b) (c)

Figure 11: Roll angle and steering angle of the "8"-shape trajectory tracking. (a) Rear wheel contact point body-frame velocities v_{rx} and v_{ry}. (b) Roll angle φ. (b) Steering angle ϕ.

5 Path-Following Control System Design

In this section, we extend the previous modeling and control design for path-following. We extend the modeling approach in the previous section by using a coupled longitudinal and lateral friction forces in tire/road interaction modeling. We also introduce a velocity-field maneuver regulation control in which the goal of the control system design is to follow the trajectory path, while the desired vehicle velocity is self-tuned online.

5.1 Modeling of tire/road friction forces

In Section 3, we presented a piecewise linear approximate of the motorcycle tire/road friction forces. However, the dependency and coupling effects between the longitudinal and lateral forces are not considered. We extend

the previous results and present a coupled friction force model here.

We consider the pseudo-static friction model of the longitudinal force F_x and longitudinal slip ratio λ_s, and the lateral force F_y and side slip ratio λ_γ ($\lambda_\gamma = \tan\gamma$, γ is slip angle). We propose to approximate the friction forces by a piecewise linear relationship given by (29). To capture the coupling effects between F_x and F_y, we consider the model parameters k and x_m along the x and y directions are dependent on each other. For example, the values of the longitudinal stiffness k_x (i.e., k value in (29) for F_x) and the maximum slip ratio λ_{sm} (i.e., x_m value in (29) for F_x) are functions of tire slip angle ratio λ_γ. Similarly, tire corning stiffness k_y (i.e., k value in (29) for F_y) and the maximum side slip ratio $\lambda_{\gamma m}$ (i.e., x_m value in (29) for F_y) also depend on the longitudinal slip ratio λ_s. Denoting k_{0x} and λ_{sm0} (k_{0y} and $\lambda_{\gamma m0}$) as the parameter values of longitudinal (lateral) force F_x (F_y) when coupling effects with F_y (F_x) are not considered, we use the following equations to update parameters k_x and λ_{sm} (parameters k_y and $\lambda_{\gamma m}$.). For longitudinal direction, we have

$$k_x = k_{0x}(a_1\lambda_\gamma + 1), \quad \lambda_{sm} = \lambda_{sm0} \tag{62}$$

and for lateral direction force,

$$k_y = k_{0y}\frac{a_2\lambda_s + 1}{a_3\lambda_s + 1}, \quad \lambda_{\gamma m} = (a_3\lambda_s + 1)\lambda_{\gamma m0}, \tag{63}$$

where a_1, a_2, and a_3 are three parameters in the coupled tire model. We use (62) and (63) to capture the coupling friction force effects because such relationships have been observed in experiments.

Figure 12 shows the property of the coupled tire mode when $k_{x0} = 30000$ N and $k_{y0} = 24000$ N. In this example, we use $a_1 = -\frac{5}{3}$, $a_2 = -2$, and $a_3 = 10$ for the motorcycle tires. For slip ratio λ_s, we set $\lambda_{sm0} = 0.15$, $\lambda_{\max} = 0.5$, $\alpha_x = 0.8$; and for side slip ratio λ_γ, we set $\lambda_{\gamma m0} = 0.11$, $x_{\max} = 1$,$\alpha_x = 0.9$.

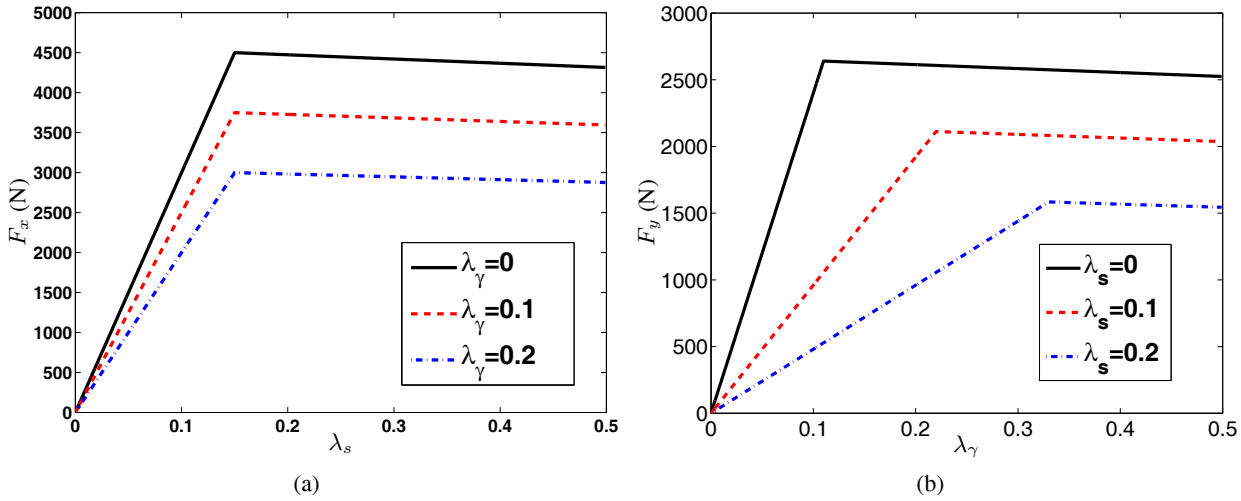

Figure 12: Approximate piecewise linear tire forces characteristics. (a) Longitudinal force with various tire slip angle ratios λ_γ. (b) Lateral force with various tire slip ratios λ_s. The tire stiffness parameters are from [37].

5.2 Combined motorcycle and tire dynamics model

We combine the above motorcycle dynamics with the tire friction force models. The controlled input variables are considered to be the front and rear wheel angular velocities ω_f and ω_r and the steering angle ϕ. We re-write the longitudinal forces at the front and rear wheels similar to (33) and (34), respectively. However, the corresponding forces in (33) and (34) are $F_{1i} = k_{i\lambda}a_{1i\lambda}$, $F_{2i} = k_{i\lambda}a_{2i\lambda}$, $F_{1i} = k_{i\lambda}a_{1i\lambda}$, $F_{2i} = k_{i\lambda}a_{2i\lambda}$, $i = f, r$, where $a_{ji\lambda}$, $a_{ji\gamma}$, $j = 1, 2$, are the longitudinal and lateral force model parameters defined in (29), respectively. $\lambda_{\gamma eq}$ is the equivalent side slip ratio developed in Section 3.

Plugging (33) and (34) into (21) and using the relationship (29), we obtain

$$\mathbf{M}(\boldsymbol{q}, \sigma)\ddot{\boldsymbol{q}} = \mathbf{K}(\dot{\boldsymbol{q}}, \boldsymbol{q}, \sigma) + \mathbf{B}\boldsymbol{u}, \tag{64}$$

where input $\boldsymbol{u} := \begin{bmatrix} \omega_\sigma & \boldsymbol{u}_\lambda^T \end{bmatrix}^T$, $\boldsymbol{u}_\lambda = \begin{bmatrix} \lambda_{fs} & \lambda_{rs} \end{bmatrix}^T$, which depends on wheel velocities. Matrix

$$\mathbf{K} = \begin{bmatrix} (K_m)_1 \\ \hdashline (K_m)_2 - \dfrac{F_{1f}}{m\sqrt{1+\sigma^2}} - \dfrac{\sigma}{m\sqrt{1+\sigma^2}} F_{34} + \dfrac{F_{1r}}{m} \\ (K_m)_3 - \dfrac{\sigma F_{1f}}{m\sqrt{1+\sigma^2}} + \dfrac{1}{m\sqrt{1+\sigma^2}} F_{34} - \dfrac{F_{ry}}{m} \end{bmatrix},$$

$(K_m)_i$ is the ith row of matrix $\mathbf{K}_m$, $F_{34} = F_{3f} + F_{4f}\left[\lambda_{f\gamma} + \frac{k_{f\varphi}}{k_{f\gamma}}(2\sigma - \lambda_{r\gamma})\right]$, and

$$\mathbf{B} = \left[\begin{array}{c:cc} -\dfrac{bh}{l} c_\varphi v_{rx} & 0 & 0 \\ \hdashline B_\omega + \dfrac{r\sigma F_{4f} \tan\xi c_\varphi^2 k_{f\varphi}}{m v_{rx} k_{f\gamma}\sqrt{1+\sigma^2}} & -\dfrac{F_{2f}}{m\sqrt{1+\sigma^2}} & \dfrac{F_{2r}}{m} \\ -\dfrac{b v_{rx}}{l} - \dfrac{r F_{4f} \tan\xi c_\varphi^2 k_{f\varphi}}{m v_{rx} k_{f\gamma}\sqrt{1+\sigma^2}} & -\dfrac{\sigma F_{2f}}{m\sqrt{1+\sigma^2}} & 0 \end{array}\right].$$

5.3 Path-Following Maneuvering Design

We propose to use velocity field-based approach to design the path-following control of the motorcycle system. We assume that the motorcycle motion planning modules such as the one in [40] generate the desired trajectory $\mathcal{T}$: $(X_d(\tau), Y_d(\tau))$. Note that the trajectory $\mathcal{T}$ is parameterized by τ, which is not necessarily the same as the time variable t. Therefore, the desired outcome of the control design design is to follow the trajectory path without specifying the velocity trajectory associated with the path. Instead, the desired velocity profile is a part of the control design process using a time-suspension technique.

5.3.1 Time suspension and velocity field design

We use a time suspension technique to design the desired velocity profile. The basic idea of time suspension is to use self-placing technique to adjust the desired rate of the progression of the parameter τ related to the desired trajectory $\mathcal{T}$. In other word, we do not need to assign any desired velocity profile in advance and the motorcycle can instantaneously adjust its velocity according to the changes of the path-following errors. One obvious advantage of using the time suspension technique in our design is to reduce tracking error and thus improve tracking performance.

We also use a velocity field design concept. The adopted velocity field approach is to define a reference input as a vector of velocities in the moving plane, rather than directly in terms of a reference-parameterized path. The main benefit of using a velocity field design is to eliminate the radial reduction phenomenon where the radius of the actual contour is smaller than the desired one [32]. To analytically construct the velocity field, we use a potential function-based approach that is similar to those in [32]. We define the following potential function to capture the position errors along the path.

$$U(X,Y) = \frac{1}{2}\beta_1 \left[(1 - \cos(X - X_d)) + (1 - \cos(Y - Y_d))\right], \tag{65}$$

where $\beta_1 > 0$ is a constant gain. At any position, we design the velocity vector by

$$\begin{bmatrix} V_x(\tau) \\ V_y(\tau) \end{bmatrix} = \lambda_1(X,Y) \begin{bmatrix} \frac{dX_d}{d\tau} \\ \frac{dY_d}{d\tau} \end{bmatrix} - \lambda_2(X,Y) \begin{bmatrix} h\sin(X - X_d) \\ h\sin(Y - Y_d) \end{bmatrix}, \tag{66}$$

where $\lambda_1(X,Y) = e^{-\beta_2 U(X,Y)}$, $\lambda_2(X,Y) = 2 - e^{-\beta_2 U(X,Y)}$, and $\beta_2 > 0$ is a self-pacing parameter. The time suspension level is defined by the following dynamics of τ

$$\dot{\tau} = \frac{d\tau}{dt} = \lambda_1(X,Y). \tag{67}$$

Remark 5 *We consider the time suspension parameter dynamics (67) as a part of augmented motorcycle dynamics (64). Note that the τ dynamics is related to the potential function $U(X,Y)$ and therefore the path following errors. When the motorcycle follows the desired trajectory, $U(X,Y) = 0$ and $\dot{\tau} = 1$. In this case, τ can be considered as the time variable t. When the path-following errors are large, the progression of desired trajectory (i.e., $\dot{\tau}$) is reduced and the controlled trajectory converges to desired path soon with increased $\lambda_2(X,Y)$. It is noted that $0 < \lambda_1(X,Y) \leq 1$ and $1 \leq \lambda_2(X,Y) < 2$.*

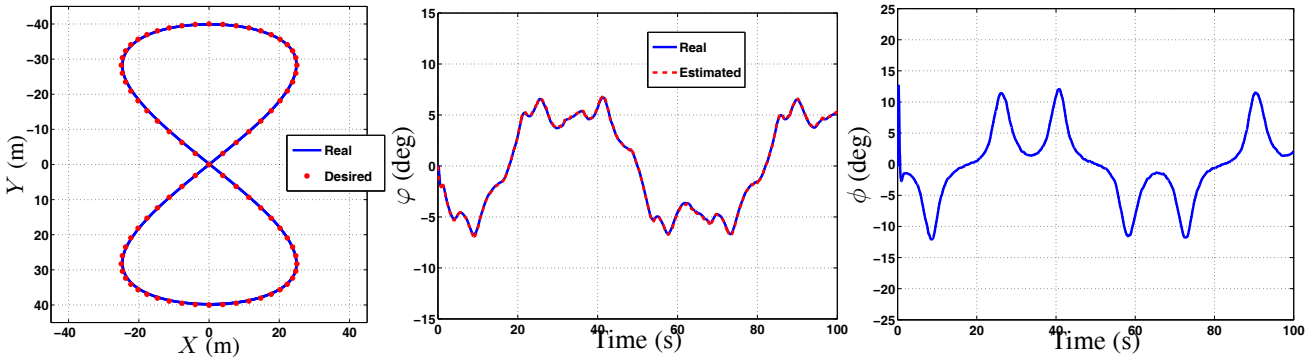

(a) (b) (c)

Figure 13: (a) Trajectory tracking. (b) Roll angle φ. (c) Steering angle ϕ.

5.3.2 Controller Design

For motorcycle control systems design, we combine the external/internal convertible (EIC) control approach discussed in the previous section with the above discussed velocity field approach.

The EIC-based trajectory control design consists of two steps; see Fig. 6. We assume that in EIC design the desired trajectory $\mathcal{T}$: $(X_d(t), Y_d(t))$ is at least $\mathcal{C}^4$, namely, differentiable at least to fourth order. The velocity vector parameterized by τ, rather than desired trajectory path specified in time t, is used as the reference input to the EIC control. We combine the EIC control and the velocity field design as follows. At any position and on any particular τ, we use (65) and (66) to calculate the current velocity vector. Then we construct a special trajectory for the EIC controller as

$$\begin{bmatrix} X_d(\tau) \\ X_d^1(\tau) \\ X_d^{(2,4)}(\tau) \end{bmatrix} = \begin{bmatrix} X(\tau) \\ V_x(\tau) \\ 0 \end{bmatrix}, \quad \begin{bmatrix} Y_d(\tau) \\ Y_d^1(\tau) \\ Y_d^{(2,4)}(\tau) \end{bmatrix} = \begin{bmatrix} Y(\tau) \\ V_y(\tau) \\ 0 \end{bmatrix},$$

where τ is updating by (66). The basic design idea is to let velocity vector be the only desired components in desired trajectory space. With this treatment, we can fully inherit the EIC controller design and its properties that are stated in [33].

5.4 Simulation Results

In this section, we demonstrate the control systems design through two examples: one is for a typical "8"-shape trajectory following maneuver and the other for a more agile maneuver. We use the same racing motorcycle and tire profiles in the simulation as these in the previous section.

The first example shows that the motorcycle runs under a regular "8"-shape path following maneuver in which the motorcycle turns along trajectory with relative large curvatures. The desired parameterized trajectory (see Fig. 13(a)) is given by the following equation parameterized by τ

$$\begin{bmatrix} X_d(\tau) \\ Y_d(\tau) \end{bmatrix} = \begin{bmatrix} 25\sin(0.1\pi\tau) \\ 40\cos(0.05\pi\tau) \end{bmatrix} \tag{68}$$

Figure 13 shows the simulation results. As shown in Fig. 13(a), the starting point of motorcycle is $(0, 40)$. We use the self-pacing parameter $\beta_2 = 100$ in (66), the parameter $\beta_1 = 0.0025$ in (65), and the initial velocity is 0.1 m/s. In the simulation, we add white noise with standard variations 0.02 m/s, 0.005 m/s^2, 0.3 deg., and 0.6 deg to velocity, acceleration, roll angle, and yaw angle measurements, respectively. By comparing with the desired trajectory, the simulation results show that the motorcycle can successfully track the desired trajectory under the velocity field control. Figure 13(b) and 13(c) clearly shows the desired and actual motorcycle roll angle φ and steering angle ϕ, respectively. The roll angle and steering angle are relatively large when turning around a small radius curvature and small in straight line.

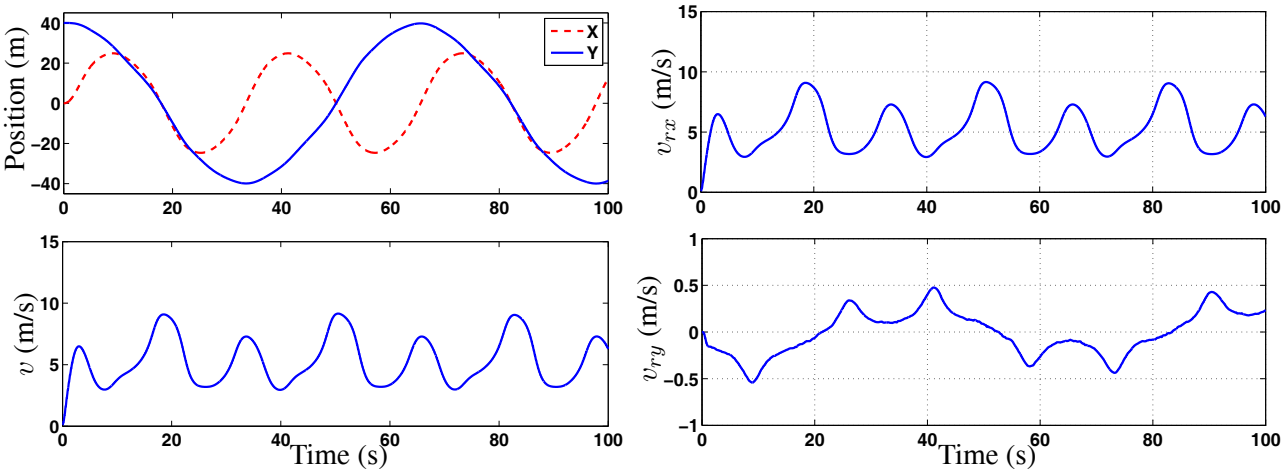

(a) (b)

Figure 14: A typical motorcycle path-following maneuver. (a) Motorcycle position and velocity (b) Longitudinal velocity v_{rx} and lateral velocity v_{ry}

Figure 14 shows the X- or Y-axis positions, longitudinal velocity and lateral velocity of rear wheel contact point C_2. From Fig. 14(a), the motorcycle spends about 65 s to go through one entire circle. It is quite clear that the motorcycle tunes its own velocity automatically using the self-placing technique. When tuning at a small radius, the tracking errors become large. The motorcycle control system then reduces the rate of the progression in time, namely, its longitudinal velocity, to reduce the errors. Meanwhile, due to the sharply direction change, the lateral velocity is relatively large; see Fig. 14(b).

The tire slip ratios and angles during the maneuver are shown in Fig. 15. For the front wheel, we see a maximum 15-degree side slip angle. For the rear wheel, the slip angle reaches almost 6 degrees, which is around the saturation point of the tire characteristics (Table 1). The longitudinal slip ratios are relatively small since the longitudinal accelerations of the motorcycle are not large and the racing motorcycle tire is stiff. At the starting point, due to the large gap between desired velocity vector and initial velocity and the large acceleration, the longitudinal slip is obvious larger than that under normal running conditions.

Figure 16(a) shows the tracking error performances of the motorcycle under different values of self-pacing parameter β_2. From this figure, we can see that when self-pacing is increased (i.e., increasing β_2), the tracking errors become smaller, namely, the better path-following performance. When $\beta_2 = 0$, the maximal error is always smaller than 0.3 m. Of course, the better performance is trade-off by the lower motorcycle velocity. This

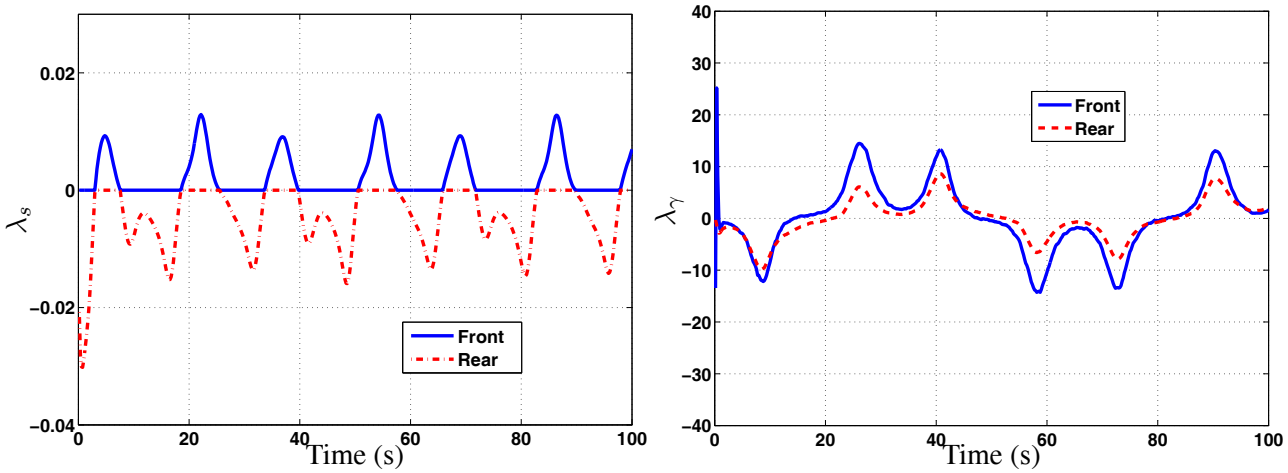

(a) (b)

Figure 15: Slip ratios and angles at the front and rear wheels during the "8"-shape trajectory tracking. (a) Slip ratio λ_s. (b) Slip angles γ_γ.

can be observed by the progression factor $\dot{\tau}$ as shown in Fig. 16(b). From Fig. 16(b), we see that increasing β_2 will reduce the value of $\dot{\tau}$ in general, which implies that the time has been expanded more since $\dot{\tau}$ is smaller. We can clearly see when $\beta_2 = 0$, $\dot{\tau} = 1$ and then the progression always remains at one, which implies no time suspension exists. In this case, the path-following system is the same as time-based trajectory tracking as shown in the previous section. Note that the oscillation of both path-following errors and progression $\dot{\tau}$ are due to the repeated motion trajectory.

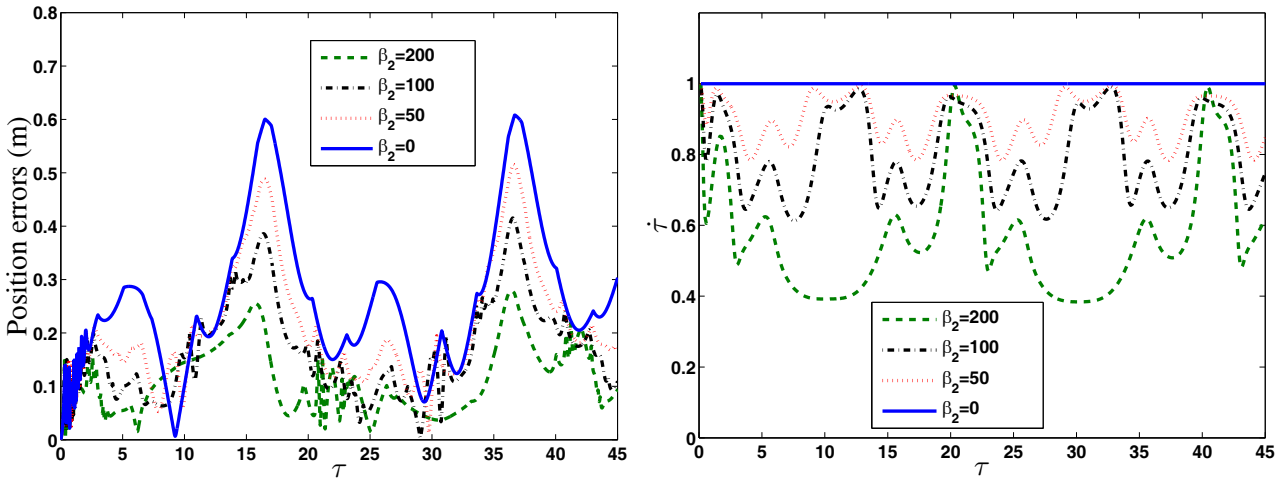

(a) (b)

Figure 16: (a) Path-following errors under various values of self-pacing parameter β_2. (b) Progression (i.e., $\dot{\tau}$) under various values of self-pacing parameter β_2.

In the second example, we show that the motorcycle runs with a more agile "8"-shape path-following maneuver. In this maneuver, the motorcycle will turn sharply at much smaller radii. The desired parameterized trajectory as shown in Fig. 17(a) is defined as

$$\begin{bmatrix} X_d(\tau) \\ Y_d(\tau) \end{bmatrix} = \begin{bmatrix} 7.5\sin(0.5\pi\tau) \\ 15\cos(0.25\pi\tau) \end{bmatrix} \tag{69}$$

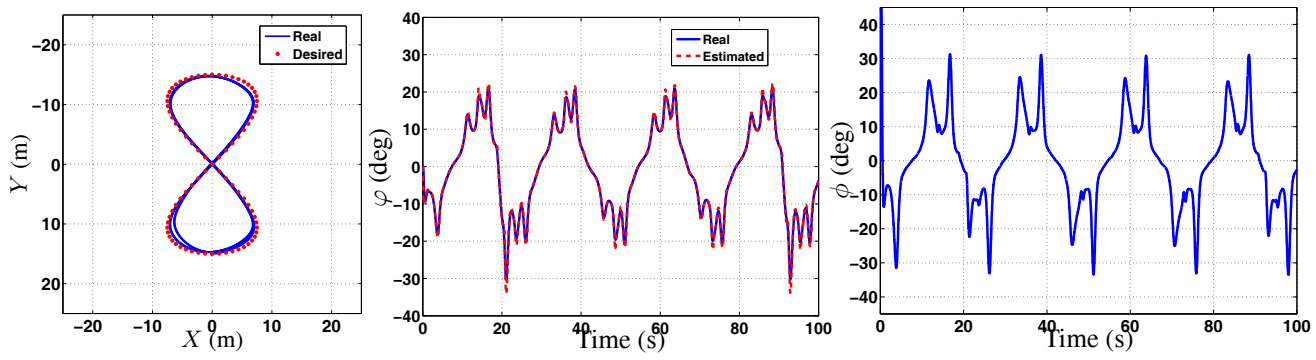

(a) (b) (c)

Figure 17: Motorcycle agile motion. (a) Path-following performance. (b) Roll angle φ. (c) Steering angle ϕ.

The start point of motorcycle is $(0, 15)$. We choose the self-pacing parameter $\beta_2 = 80$ and the parameter $\beta_1 = 0.00825$. The initial velocity and noise characteristics are the same as those in the previous example.

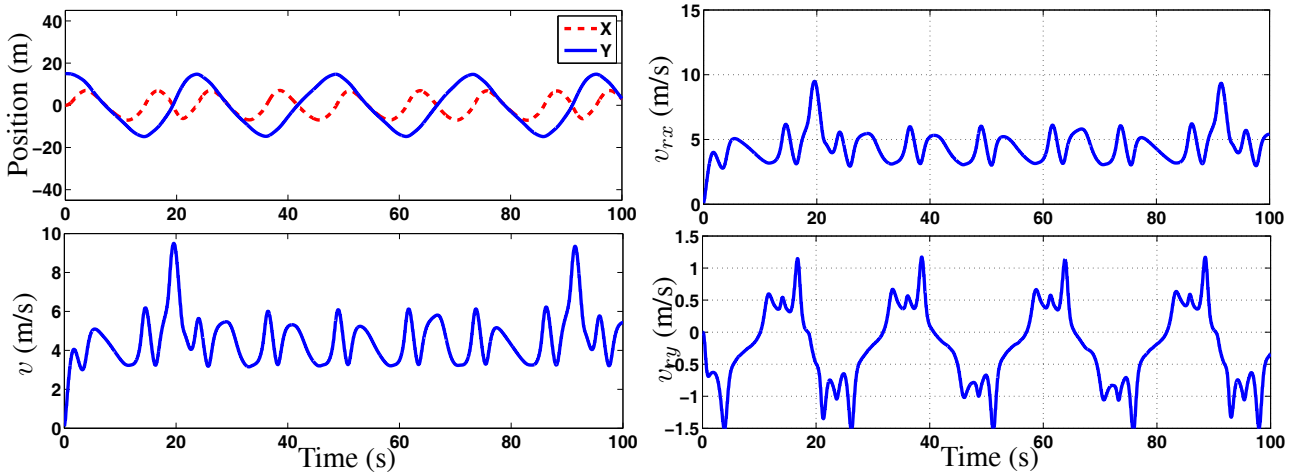

(a) (b)

Figure 18: Motorcycle agile maneuver. (a) Position and velocity (b) Longitudinal velocity and lateral velocity

From Fig. 17(a), we see that even in this extreme case the motorcycle can still follow the desired trajectory under the velocity field control. From Fig. 17(b) and 17(c), it is clear that the steering angle and roll angle are both obvious larger than those of the previous example due to the much smaller radius curvatures. Figure 18(a) and 18(b) show the motorcycle position and velocity information for this maneuver. We see a large lateral velocity v_{ry}. Figure 19(a) and 19(b) show the tire slip ratios and slip angles, respectively. It is noted from Fig. 19(a) that the required longitudinal slip ratio of the rear tire can nearly reach 0.15, which is nearly the maximal stable slip ratio of the tire model. From Fig. 19(b), we also see the large slip angles under this agile maneuver.

We clearly see a large side slip angles shown in Fig. 20(b). Particularly, for the front wheel, we have seen a 15 degree side slip angle. For the rear wheel, the side slip angle reaches almost 6 degrees, which is around the saturation point of the tire characteristics (Table 1). In other words, the motorcycle rear wheel is starting to slide on the ground. If the side slip angle increases further, the stability of the motorcycle will change significantly. The longitudinal slip are relatively small since the longitudinal acceleration of the motorcycle is not large and the racing motorcycle tire is stiff. This simulation example demonstrates that the proposed dynamic model and control systems capture the realistic aggressive motorcycle maneuvers.

Comparing with time-based trajectory tracking control design in the previous section, the simulation results show that the velocity field based path-following design achieves smoother velocity profiles and much smaller

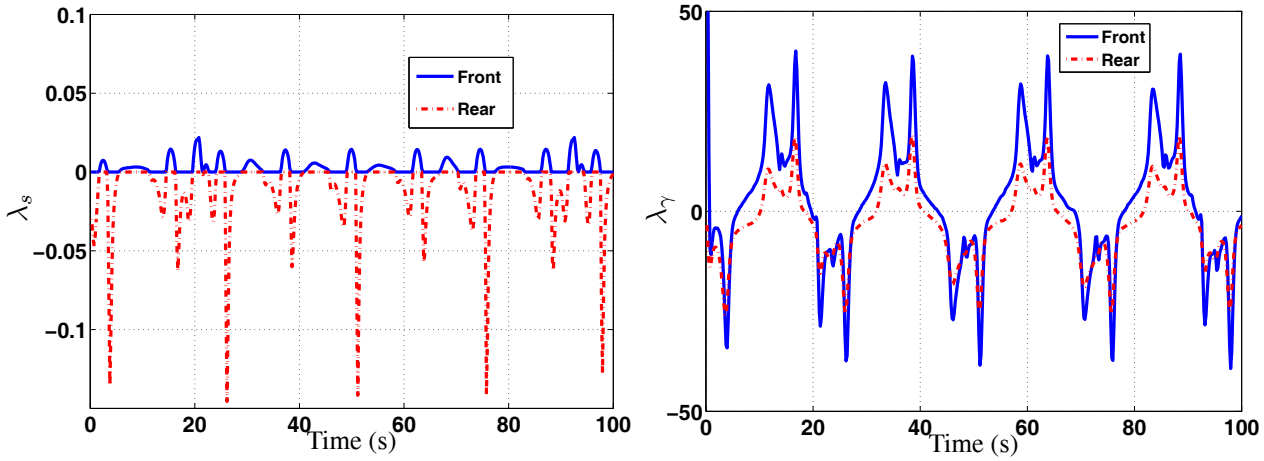

(a) (b)

Figure 19: Slip ratios and angles under the agile maneuver. (a) Slip ratio λ_s. (b) Slip angles λ_γ.

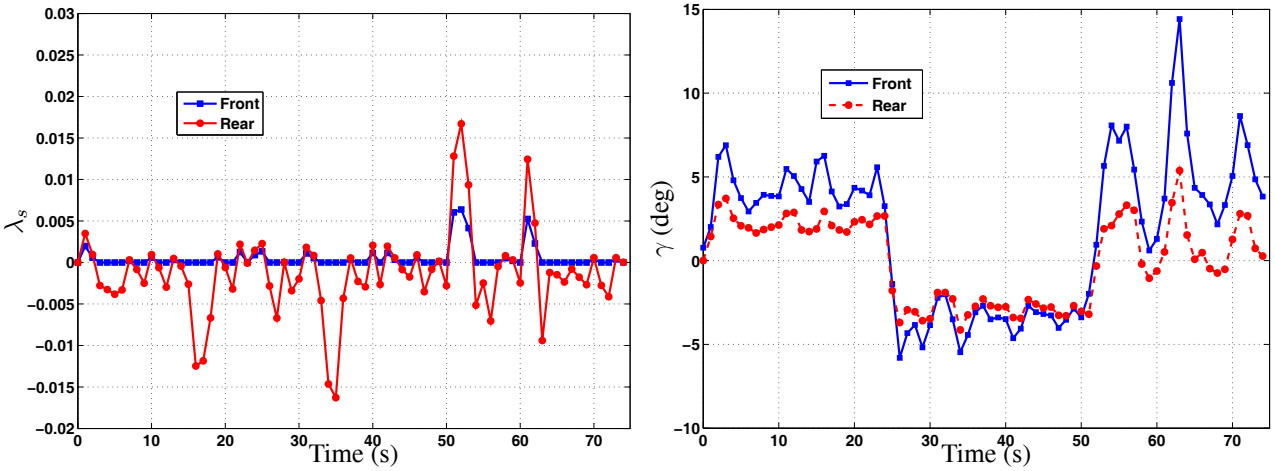

(a) (b)

Figure 20: Longitudinal slips and slip angles at the front and rear wheels of the "8"-shape trajectory tracking. (a) Slip ratio λ_{fs} and λ_{rs}. (b) Slip angles γ_f and γ_r.

tracking errors.

6 Conclusion

In this report, we presented a new nonlinear dynamic model and tracking control for autonomous motorcycles/bicycles. The proposed dynamic model is obtained through a constrained Lagrange modeling approach. Comparing with the existing riderless motorcycle models, the new features of the proposed motorcycle dynamics model are twofold: First, we relaxed the assumption of zero-lateral-velocity constraints at tire contact points and thus the model can be used for the agile maneuvers when wheels run with large longitudinal slips and lateral side slips. Second, we considered the motorcycle tire models and extended previously developed motorcycle dynamics. Both trajectory tracking and path-following control are presented for agile maneuvers. The nonlinear trajectory tracking control design takes advantages of the external/internal convertible (EIC) dynamical structure of the motorcycle dynamics. We extend the EIC design to the three control inputs case and such extension allows flexibility in control systems design and therefore simplifies the complexity of the final calculation. We have demonstrated the trajectory tracking control systems design through two simulation examples using a racing

motorcycle prototype. To improve the tracking performance, we further presented a velocity field based path-following control design of an autonomous motorcycle system. We combined the velocity field design with the previously developed EIC motorcycle controller. The control system can automatically tune the velocity profile based on the tracking errors and trajectory properties. The simulation results of a typical maneuver and an agile maneuver have demonstrated that the velocity field based path-following control design improved the tracking errors.

There are several ongoing research directions. We are currently implementing the proposed control systems on a Rutgers autonomous motorcycle platform. We will report the implementation results in the near future. Moreover, we also plan to study how the professional racing drivers control motorcycles for agile maneuvers.

Acknowledgments

The first author thanks Dr. N. Getz at Inversion Inc. for his helpful suggestions and support. The authors are grateful to Prof. S. Jayasuriya at the University of Central Florida, Dr. E.H. Tseng and Dr. J. Lu at Ford Research and Innovation Center for their helpful discussions and suggestions.

References

[1] A. Levandowski, A. Schultz, C. Smart, A. Krasnov, H. Chau, B. Majusiak, F. Wang, D. Song, J. Yi, H. Lee, and A. Parish, "Ghostrider: Autonomous motorcycle," in *Proc. IEEE Int. Conf. Robot. Autom. (Video)*, Orlando, FL, 2006.

[2] D. Limebeer and R. Sharp, "Bicycles, motorcycles, and models," *IEEE Control Syst. Mag.*, vol. 26, no. 5, pp. 34–61, 2006.

[3] K. Åström, R. Klein, and A. Lennartsson, "Bicycle dynamics and control," *IEEE Control Syst. Mag.*, vol. 25, no. 4, pp. 26–47, 2005.

[4] J. Lowell and H. McKell, "The stability of bicycles," *Amer. J. Phys.*, vol. 50, no. 12, pp. 1106–1112, 1982.

[5] R. Sharp, "Stability, control and steering responses of motorcycles," *Veh. Syst. Dyn.*, vol. 35, no. 4-5, pp. 291–318, 2001.

[6] V. Cossalter and R. Lot, "A motorcycle multi-body model for real time simulations based on the natural coordinates approach," *Veh. Syst. Dyn.*, vol. 37, no. 6, pp. 423–447, 2002.

[7] V. Cossalter, *Motorcycle Dynamics*. Greendale, WI: Race Dynamics, 2002.

[8] P. Kessler, "Motorcycle navigation with two sensors," Master's thesis, Dept. Mech. Eng., Univ. California, Berkeley, CA, 2004.

[9] N. Getz, "Dynamic inversion of nonlinear maps with applications to nonlinear control and robotics," Ph.D. dissertation, Dept. Electr. Eng. and Comp. Sci., Univ. Calif., Berkeley, CA, 1995.

[10] R. Sharp, "The stability and control of motorcycles," *J. Mech. Eng. Sci.*, vol. 13, no. 5, pp. 316–329, 1971.

[11] F. Biral, D. Bortoluzzi, V. Cossalter, and M. Da Lio, "Experimental study of motorcycle transfer functions for evaluating handling," *Veh. Syst. Dyn.*, vol. 39, no. 1, pp. 1–25, 2003.

[12] D. Jones, "The stability of the bicycle," *Phys. Today*, vol. 23, no. 4, pp. 34–40, 1970.

[13] J. Fajans, "Steering in bicycles and motorcycles," *Amer. J. Phys.*, vol. 68, no. 7, pp. 654–659, 2000.

[14] V. Cossalter, R. Lot, and F. Maggio, "The modal analysis of a motorcycle in straight running and on a curve," *Meccanica*, vol. 39, pp. 1–16, 2004.

[15] J. Meijaard, J. Papadopoulos, A. Ruina, and A. Schwab, "Linearized dynamics equations for the balance and steer of a bicycle: A benchmark and review," *Proc. Royal Soc. A*, vol. 463, pp. 1955–1982, 2007.

[16] J. Yi, D. Song, A. Levandowski, and S. Jayasuriya, "Trajectory tracking and balance stabilization control of autonomous motorcycles," in *Proc. IEEE Int. Conf. Robot. Autom.*, Orlando, FL, 2006, pp. 2583–2589.

[17] A. Beznos, A. Formal'sky, E. Gurfinkel, D. Jicharev, A. Lensky, K. Savitsky, and L. Tchesalin, "Control of autonomous motion of two-wheel bicycle with gyroscopic stabilisation," in *Proc. IEEE Int. Conf. Robot. Autom.*, Leuven, Belgium, 1998, pp. 2670–2675.

[18] S. Lee and W. Ham, "Self-stabilzing strategy in tracking control of unmanned electric bicycle with mass balance," in *Proc. IEEE/RSJ Int. Conf. Intell. Robot. Syst.*, Lausanne, Switzerland, 2002, pp. 2200–2205.

[19] Y. Tanaka and T. Murakami, "Self sustaining bicycle robot with steering controller," in *Proc. 2004 IEEE Adv. Motion Contr. Conf.*, Kawasaki, Japan, 2004, pp. 193–197.

[20] ——, "A study on straight-line tracking and posture control in electric bicycle," *IEEE Trans. Ind. Electron.*, vol. 56, no. 1, pp. 159–168, 2009.

[21] R. Lot, "A motorcycle tires model for dynamic simulations : Theoretical and experimental aspects," *Meccanica*, vol. 39, pp. 207–220, 2004.

[22] J. Hauser and A. Saccon, "Motorcycle modeling for high-performance maneuvering," *IEEE Control Syst. Mag.*, vol. 26, no. 5, pp. 89–105, 2006.

[23] J. Yi, Y. Zhang, and D. Song, "Autonomous motorcycles for agile maneuvers: Part I: Dynamic modeling," in *Proc. IEEE Conf. Decision Control*, Shanghai, China, 2009, pp. 4613–4618.

[24] F. Bullo and A. Lewis, *Geometric Control of Mechanical Systems: Modeling, Analysis, and Design for Simple Mechanical Control Systems*. New York, NY: Springer, 2004.

[25] S. Sastry, *Nonlinear Systems: Analysis, Stability, and Control*. New York, NY: Springer, 1999.

[26] J. Grizzle, M. Di Benedetto, and F. Lamnabhi-Lagarrigue, "Necessary conditions for asymptotic tracking in nonlinear systems," *IEEE Trans. Automat. Contr.*, vol. 39, no. 9, pp. 1782–1794, 1994.

[27] J. Hauser and R. Hindman, "Maneuver regulation from trajectory tracking: Feedback linearizable systems," in *Proc. IFAC Symp. Nonlinear Contr. Syst. Design*, Tahoe City, CA, 1995, pp. 638–643.

[28] S. Al-Hiddabi and N. McClamroch, "Tracking and maneuver regulation control for nonlinear nonminimum phase systems: Application to flight control," *IEEE Trans. Contr. Syst. Technol.*, vol. 10, no. 6, pp. 780–792, 2002.

[29] R. Skjetne, T. Fossen, and P. Kokotović, "Robust output maneuvering for a class of nonlinear systems," *Automatica*, vol. 40, pp. 373–383, 2004.

[30] A. Aguiar, J. Hespanda, and P. Kokotović, "Path-following for nonminimum phase systems removes performance limitations," *IEEE Trans. Automat. Contr.*, vol. 50, no. 2, pp. 234–239, 2005.

[31] A. Aguiar and J. Hespanda, "Trajectory-tracking and path-following of underactuated autonomous vehicles with parametric modeling uncertainty," *IEEE Trans. Automat. Contr.*, vol. 52, no. 8, pp. 1362–1379, 2007.

[32] P. Y. Li and R. Horowitz, "Passive velocity field control (PVFC): Part II – Application to contour following," *IEEE Trans. Automat. Contr.*, vol. 46, no. 9, pp. 1360–1371, 2001.

[33] J. Yi, Y. Zhang, and D. Song, "Autonomous motorcycles for agile maneuvers: Part II: Control systems design," in *Proc. IEEE Conf. Decision Control*, Shanghai, China, 2009, pp. 4619–4624.

[34] Y. Zhang and J. Yi, "Dynamic modeling and balance control of human/bicycle systems," in *Proc. IEEE/ASME Int. Conf. Adv. Intell. Mechatronics*, Montreal, Canada, 2010, pp. 1385–1390.

[35] A. Bloch, *Nonholonomic Mechanics and Control*. New York, NY: Springer, 2003.

[36] Y. Zhang, J. Li, J. Yi, and D. Song, "Balance control and analysis of stationary riderless motorcycles," in *Proc. IEEE Int. Conf. Robot. Autom.*, Shanghai, China, 2011, pp. 3018–3023.

[37] R. S. Sharp, S. Evangelou, and D. J. N. Limbeer, "Advances in the modelling of motorcycle dynamics," *Multibody Syst. Dyn.*, vol. 12, pp. 251–283, 2004.

[38] A. Isidori, *Nonlinear Control Systems*, 3rd ed. London, UK: Springer-Verlag, 1995.

[39] J. C. Gerdes and E. J. Rossetter, "A unified approach to driver assistance systems based on artificial potential fields," *ASME J. Dyn. Syst., Meas., Control*, vol. 123, no. 3, pp. 431–438, 2001.

[40] D. Song, H.-L. Lee, J. Yi, and A. Levandowski, "Vision-based motion planning for an autonomous motorcycle on ill-structured roads," *Auton. Robots*, vol. 23, no. 3, pp. 197–212, 2007.

[41] M. Corno, S. M. Savaresi, M. Tanelli, and L. Fabbri, "On optimal motorcycle braking," *Contr. Eng. Pract.*, vol. 16, pp. 644–657, 2008.

A Calculation of M_s

We consider the front wheel center O_1 and the projected steering axis point C_3 on the ground surface. Since the frictional moment is independent of the coordinate system. We can setup a local coordinate system $x_f y_f z_f$ by rotating the coordinate system xyz around the z-axis with an angle ϕ_g (origin at contact point C_1). Let $(\boldsymbol{i}_f, \boldsymbol{i}_f, \boldsymbol{i}_f)$ denote the unit vectors along the x_f, y_f, z_f-axis directions, respectively.

In the new coordinate system, we obtain the coordinates of O_1 and C_3 as $(0, r\,\mathrm{s}_{\varphi_f}, -r\,\mathrm{c}_{\varphi_f})$ and $(l_t, 0, 0)$, respectively. We write the front wheel friction force vector $\boldsymbol{F}_f$ as

$$\boldsymbol{F}_f = -F_{fx}\boldsymbol{i}_f - F_{fy}\boldsymbol{j}_f - F_{fz}\boldsymbol{k}_f$$

and the vector $\boldsymbol{r}_{C_3C_1} = -l_t\boldsymbol{i}_f$. The directional vector $\boldsymbol{n}_{O_1C_3}$ of the steering axis O_1, C_3 is then

$$\boldsymbol{n}_{O_1C_3} = \frac{l_t\boldsymbol{i}_f - r\,\mathrm{s}_{\varphi_f}\boldsymbol{j}_f + r\,\mathrm{c}_{\varphi_f}\boldsymbol{k}_f}{\sqrt{l_t^2 + r^2}}.$$

Therefore, the friction moment M_s about the steering axis is calculated as

$$M_s = (\boldsymbol{r}_{C_3C_1} \times \boldsymbol{F}_f) \cdot \boldsymbol{n}_{O_1C_3} = \frac{l_t}{\sqrt{1 + (l_t/r)^2}} \left(F_{fy}\,\mathrm{c}_{\varphi_f} - F_{fz}\,\mathrm{s}_{\varphi_f}\right).$$

B Calculation of acceleration $\dot{\boldsymbol{v}}_G$

Taking the time derivative of the mass center velocity $\boldsymbol{v}_G$ and considering the moving frame xyz's angular velocity $\boldsymbol{\omega} = \dot{\varphi}\boldsymbol{i} + \dot{\psi}\boldsymbol{k}$, we obtain

$$\begin{aligned}
\dot{\boldsymbol{v}}_G = \frac{\delta \boldsymbol{v}_G}{\delta t} + \boldsymbol{\omega} \times \boldsymbol{v}_G &= (\dot{v}_{rx} - h\ddot{\psi}\,\mathrm{s}_\varphi - h\dot{\psi}\dot{\varphi}\,\mathrm{c}_\varphi)\boldsymbol{i} + (\dot{v}_{ry} + b\ddot{\psi} + h\ddot{\varphi}\,\mathrm{c}_\varphi \\
&\quad - h\dot{\varphi}^2\,\mathrm{s}_\varphi)\boldsymbol{j} + (h\ddot{\varphi}\,\mathrm{s}_\varphi + h\dot{\varphi}^2\,\mathrm{c}_\varphi)\boldsymbol{k} + (\dot{\varphi}\boldsymbol{i} + \dot{\psi}\boldsymbol{k}) \times \boldsymbol{v}_G \\
&= (\dot{v}_{rx} - v_{ry}\dot{\psi} - h\ddot{\psi}\,\mathrm{s}_\varphi - b\dot{\psi}^2 - 2h\dot{\psi}\dot{\varphi}\,\mathrm{c}_\varphi)\boldsymbol{i} + (\dot{v}_{ry} + v_{rx}\dot{\psi} + b\ddot{\psi} + h\ddot{\varphi}\,\mathrm{c}_\varphi - h\dot{\psi}^2\,\mathrm{s}_\varphi \\
&\quad - 2h\dot{\varphi}^2\,\mathrm{s}_\varphi)\boldsymbol{j} + (v_{ry}\dot{\varphi} + h\ddot{\varphi}\,\mathrm{s}_\varphi + b\dot{\psi}\dot{\varphi} + 2h\dot{\varphi}^2\,\mathrm{c}_\varphi)\boldsymbol{k},
\end{aligned}$$

where $\frac{\delta \boldsymbol{v}_G}{\delta t}$ denotes the derivative of $\boldsymbol{v}_G$ by treating the xyz-coordinate as a fixed frame.

C Calculation of the Lie derivatives

The calculation of $\bar{L}_{\mathbf{N}_{\text{ext}}} u_{rx}^{\text{ext}}$ and $\bar{L}_{\mathbf{N}_{\text{ext}}} u_{ry}^{\text{ext}}$ is obtained by taking the Lie derivative along the nominal external vector field (52) and the control input (54). The calculation are shown in (70) and (71).

$$\begin{aligned}
\bar{L}_{\mathbf{N}_{\text{ext}}} u_{rx}^{\text{ext}} &= \begin{bmatrix} -\mathrm{s}_\psi & \mathrm{c}_\psi \end{bmatrix} \dot{\psi} \left(-\mathbf{U} + \boldsymbol{u}^{\text{ext}} \right) + \begin{bmatrix} \mathrm{c}_\psi & \mathrm{s}_\psi \end{bmatrix} \\
&\quad \left(- \begin{bmatrix} -2u_{rx}^{\text{ext}}\,\mathrm{s}_\psi - 2u_{ry}^{\text{ext}}\,\mathrm{c}_\psi - 3\dot{v}_{rx}\dot{\psi}\,\mathrm{c}_\psi + 3\dot{v}_{ry}\dot{\psi}\,\mathrm{s}_\psi + \ddot{\psi}\left(v_{rx}\,\mathrm{s}_\psi + v_{ry}\,\mathrm{c}_\psi\right) \\ 2u_{rx}^{\text{ext}}\,\mathrm{c}_\psi - 2u_{ry}^{\text{ext}}\,\mathrm{s}_\psi - 3\dot{v}_{rx}\dot{\psi}\,\mathrm{s}_\psi - 3\dot{v}_{ry}\dot{\psi}\,\mathrm{c}_\psi - \ddot{\psi}\left(v_{rx}\,\mathrm{c}_\psi - v_{ry}\,\mathrm{s}_\psi\right) \end{bmatrix} \dot{\psi} + \begin{bmatrix} \bar{L}_{\mathbf{N}_{\text{ext}}} u_X^{\text{ext}} \\ \bar{L}_{\mathbf{N}_{\text{ext}}} u_Y^{\text{ext}} \end{bmatrix} \right) \\
&= \dot{v}_{rx}\dot{\psi}^2 + \left(2u_{ry}^{\text{ext}} - u_X^{\text{ext}}\,\mathrm{s}_\psi + u_Y^{\text{ext}}\,\mathrm{c}_\psi\right)\dot{\psi} + \bar{L}_{\mathbf{N}_{\text{ext}}} u_X^{\text{ext}}\,\mathrm{c}_\psi + \bar{L}_{\mathbf{N}_{\text{ext}}} u_Y^{\text{ext}}\,\mathrm{s}_\psi, \qquad (70) \\
\bar{L}_{\mathbf{N}_{\text{ext}}} u_{ry}^{\text{ext}} &= \dot{v}_{ry}\dot{\psi}^2 - \left(2u_{rx}^{\text{ext}} + u_X^{\text{ext}}\,\mathrm{c}_\psi + u_Y^{\text{ext}}\,\mathrm{s}_\psi\right)\dot{\psi} - \bar{L}_{\mathbf{N}_{\text{ext}}} u_X^{\text{ext}}\,\mathrm{s}_\psi + \bar{L}_{\mathbf{N}_{\text{ext}}} u_Y^{\text{ext}}\,\mathrm{c}_\psi\,. \qquad (71)
\end{aligned}$$

In these equations, we have

$$\begin{bmatrix} \bar{L}_{\mathbf{N}_{\text{ext}}} u_X^{\text{ext}} \\ \bar{L}_{\mathbf{N}_{\text{ext}}} u_Y^{\text{ext}} \end{bmatrix} = \begin{bmatrix} X_d^{(4)}(t) \\ Y_d^{(4)}(t) \end{bmatrix} - b_3 \begin{bmatrix} u_X^{\text{ext}} - X_d^{(3)}(t) \\ u_Y^{\text{ext}} - Y_d^{(3)}(t) \end{bmatrix} - \sum_{i=1}^{2} b_i \begin{bmatrix} X^{(i)} - X_d^{(i)}(t) \\ Y^{(i)} - Y_d^{(i)}(t) \end{bmatrix}.$$

Similarly, we can calculate $\bar{L}^2_{\mathbf{N}^{\text{ext}}} \varphi_e$ by directly taking a directional derivative of $\bar{L}_{\mathbf{N}_{\text{ext}}} \varphi_e$ along the vector field $\mathbf{N}_{\text{ext}}$. From (60), we have

$$\begin{aligned}
\bar{L}^2_{\mathbf{N}_{\text{ext}}} \varphi_e = \left(h\dot{\psi}\,\mathrm{c}_{\varphi_e} + g\sec^2\varphi_e\right)^{-1} \Bigg[\frac{gbl_t\,\mathrm{c}_\xi}{h} \left(\frac{\dot{\psi} u_{rx}^{\text{ext}}}{v_{rx}^2} - \frac{2\dot{v}_{rx}^2\dot{\psi}}{v_{rx}^3} \right) + \dot{\psi} u_{rx}^{\text{ext}} + \\
\bar{L}_{\mathbf{N}_{\text{ext}}} u_{ry}^{\text{ext}} + \left(h\dot{\psi}\,\mathrm{s}_{\varphi_e} - 2g\sec^2\varphi_e \tan\varphi_e\right) \left(\bar{L}_{\mathbf{N}_{\text{ext}}} \varphi_e\right)^2 \Bigg]. \qquad (72)
\end{aligned}$$